2016

Header height control of combine harvester via robust feedback linearization

Daniel Michael Kassen
Iowa State University

Header height control of combine harvester via robust feedback linearization

by

Daniel M. Kassen

A thesis submitted to the graduate faculty

in partial fulfillment of the requirements for the degree of

MASTER OF SCIENCE

Major: Mechanical Engineering

Program of Study Committee:

Atul Kelkar, Major Professor

Brian Steward

Juan Ren

Iowa State University

Ames, Iowa

2016

DEDICATION

I would like to dedicate this thesis to my wife, Jessica, who has been a constant source of support and encouragement throughout my time at Iowa State. I am truly thankful for having you in my life. I would also like to thank my parents for always encouraging, supporting, and inspiring me to pursue and complete this work, and who have taught me to work hard for the things I aspire to achieve.

TABLE OF CONTENTS

LIST OF FIGURES

LIST OF TABLES

ACKNOWLEDGEMENTS

I would like to thank Dr. Atul Kelkar, my major professor, for his guidance, patience, and support throughout my research and writing of this thesis. I would also like to thank my committee members, Dr. Brian Steward and Dr. Juan Ren, who have generously given their time and experience to better my work. I am grateful to the graduate students, Dr. Punit Tulpule and Hui Zhou, whose previous work provided a solid base so that I may continue improving and developing the research even further.

ABSTRACT

Studies have shown that feedback linearization can provide an effective controller for many types of nonlinear systems. It is known, however, that these controllers are not robust, in particular to model uncertainties as the feedback linearization process involves canceling of nonlinearities in the dynamics using an exact model which is seldom available. Although there are several strategies to add robustness, recent work on sensitivity theory has shown that it can provide the least conservative design for robust feedback linearization. This is achieved by adjusting the control input to minimize the sensitivity. The work in this thesis develops the robust feedback linearization (RFL) methodology further by extending it to a new class of non-linear systems. This research presents a methodology for designing a RFL controller in conjunction with previous work on integrated robust optimal design (IROD) for hydraulically controlled multibody systems.

With growing world populations the total output of the agricultural industry will need to increase with it. It has been shown that a significant portion of yield losses occur during harvest, and specifically at the header of the combine harvester. One way to improve this is by improved header height tracking. Promising research has shown that integrated mechanical plant and controller design can provide a better optimal controller than previously possible, but those techniques focus on the mechanical system only and do not account for hydraulic actuator dynamics. However, in practice, hydraulic systems pose control challenges because they are highly nonlinear and the system parameters can vary significantly. The proposed RFL methodology offers an ideal solution to this problem and the work in this thesis is dedicated to developing this methodology. Details are given about the mechanical and hydraulic plants as well as the development of a nominal

feedback linearization controller. Then the controller is rendered robust to uncertainties in the bulk modulus by deriving the sensitivity dynamics and control adjustment. Finally, the controller performance is tested over a variety of simulated conditions and is compared to the current industry standard, the PID controller. The results show that the RFL controller greatly improves header height tracking with reduced input power and is robust to bulk modulus uncertainties.

CHAPTER 1. OVERVIEW AND BACKGROUND

The research presented in this thesis provides a new development and application of a newly developed control design methodology for a class of nonlinear systems. The underlying control design methodology is called Robust Feedback Linearization (RFL), which was developed in [1] as a part of doctoral research work. A sensitivity-based feedback linearization technique was proposed that can account for parametric uncertainties and the theory was demonstrated using a system consisting of a linear plant model actuated with a double acting cylinder and a 4-way spool valve. The results showed good tracking performance and that RFL can improve the robustness of the system, but due to the computationally intensive nature and assumptions made, the applicability to complex systems would be difficult. Recent graduate work presented in [2], attempted to utilize MATLAB for the symbolic derivations and Simulink for the complex physical system simulation. The methodology was demonstrated on the excavator bucket leveling control problem. Although the results showed good tracking and reduced robustness, it was not compared to another controller, so there was no measurable performance reference. Additionally, the required knowledge of valve dynamics and chosen parameters would make industry adoption doubtful. This thesis further develops the control design methodology, improves its applicability, and expands its scope to incorporate a new class of nonlinear systems. The methodology is demonstrated on a simulation of the combine harvester header height control example and its effectiveness is shown by comparing it to current industry standard classical controller.

The structure of this thesis is as follows: this chapter presents relevant background information on feedback linearization, sensitivity theory, hydraulic system control, and the combine harvester header height problem. Chapter 2 provides detailed development of the RFL methodology including control non-affine feedback linearization and sensitivity dynamics. Chapter 3 gives a generalized design strategy for designing a controller for a hydraulically controlled multibody system. Chapter 4 will demonstrate the RFL control theory and the general design strategy on the combine harvester header height example and compare the results with the PID controller. Finally, Chapter 5 will summarize the conclusions and suggestions for future research.

1.1 Robust Feedback Linearization

Feedback linearization is a control design strategy for control of nonlinear systems. The feedback linearization strategy has been effectively used for control of nonlinear systems when the system model is fairly accurate. Depending on the zero dynamics, feedback linearization may not be able to guarantee internal stability [3], but it can be used to design a controller for many difficult nonlinear systems and most types of nonlinearities. [4, 5]. A benefit over many other nonlinear methods is that it does not require determining a practical operating point. In some systems, such as with hydraulic actuators, determining an operating point outside of the dead band is not possible, so feedback linearization is an ideal choice. The basic idea behind feedback linearization is to cancel the nonlinear part of the dynamics by transforming the system through the use of a change of coordinates and a suitable control input. From here, a simple linear controller can be designed for the system, which can be tuned using standard techniques. This is another benefit over many other nonlinear control strategies, which may have control parameters that are not directly related to the performance output in an obvious way.

Even though feedback linearization has good tracking performance [6, 7] the main limitation is that it lacks robustness. Because the methodology involves canceling out the nonlinear dynamics, a detailed knowledge of the system is required. The effectiveness of the feedback linearization becomes model dependent. Early research attempted to add robustness to feedback linearization using a Lyapunov approach to account for parametric uncertainties such as in [8,9]. The Lyapnov approach has also been used more recently in [10]. The drawback of this approach is that it requires an estimate of the uncertainty bounds, which may not always be known, and could create an overly conservative controller. Another approach for robust feedback linearization is sliding mode control [11, 12]. Even though sliding mode control is robust to uncertainties, because it is based on fast switching inputs it may provide a discontinuous control input and chattering. Developments in [13] attempt to overcome this by varying boundary layers. Essentially, it is not forcing the error to zero, so even though chattering is lower, it is at the expense of tracking performance. More recent research has focused on fuzzy logic for robustification of feedback linearization. Examples of this are in [14, 15] and a literature review of other examples is given in [16].

The methodology presented in [1] proposed to use sensitivity theory to add robustness to feedback linearization. The basic concept is to minimize the sensitivity, which is defined as the change in performance as a result of perturbations in design variables. Sensitivity theory has been around for over 70 years and was first discussed in [17]. Since then it has been used in a variety of applications including sensitivity and performance optimization and robustness analysis [18]. Early research focused on LQR problems [19, 20] and proposed augmenting the sensitivity dynamics with the system equations. With the introduction of the $\mathcal{H}_\infty$ control theory by Zames in 1981 [21], which uses bounded uncertainty, sensitivity theory became less popular. The drawback of using bounded uncertainty is that it requires an estimate of the minimum and maximum values and as mentioned earlier can add unnecessary conservatism to the controller.

With advancements in technology, symbolic computation has become easier and as a result, recent research has revisited sensitivity theory for robust control applications [22]. The method proposed in [1] and developed further in this thesis provides the least conservative design by using the sensitivity dynamics to add robustness to the feedback linearization controller. This is achieved by adjusting the nominal feedback linearization calculated input slightly to minimize the sensitivity with respect to uncertain parameters. The needed adjustment is small enough such that the overall effect on the feedback linearization performance is negligible [2].

1.2 Application to Hydraulic Systems

The robust feedback linearization control design process is ideally suited for a class of nonlinear systems which cannot be linearized at an operating point. Hydraulic systems, and specifically hydraulic actuators, fall into this class and are the focus application of this research. Use of hydraulic actuators is common in industrial applications for their high load stiffness, fast response, relative low cost, and ability to operate under a variety of conditions [23, 24]. The mobile off-highway equipment industry uses fluid power extensively for the benefits mentioned above, but even more importantly for the high power density and flexible power transfer it can offer [25].

Despite the substantial use in practice, precision control of hydraulic systems has proved challenging. Hydraulics by nature are highly nonlinear with the presence of dead bands, discontinuities, square root terms in its dynamics, and other complexities [26, 27]. Even with all these nonlinearities most industry control problems are solved by linear control methods. Linearization techniques can allow for pole placement [28] and pseudo derivative feedback control [29] in electro-hydraulic servo systems. These systems may work well locally, but because it requires linearization at an operating point, the performance deteriorates as the position deviates from the operating point.

An additional challenge of hydraulic control is caused by model uncertainties. Examples of these uncertainties are: supply pressure, density, bulk modulus, and friction [30, 31]. The bulk modulus in particular is difficult and expensive to measure in practice [32] and can vary widely. The biggest factor that affects bulk modulus is entrained air. It has been shown that even 1 percent entrained air can correspond to a 75 percent decrease in bulk modulus [33]. Attempts have been made to regulate and measure bulk modulus online using an onboard vacuum degassing system in [34], but there are a number of other factors that can affect bulk modulus as well. These include temperature, pressure, and pipe compliance [35]. Hydraulic engineers often use a much lower bulk modulus than stated by the fluid supplier when designing a hydraulic system in an attempt to account for these variations.

The general design methodology presented in chapter 3 proposes a controller ideally developed for these complex hydraulic systems. The focus is on actuator functions of off-highway equipment, but could easily be expanded to other hydraulic applications. The methodology uses two separate control strategies, one for the multibody mechanical system and one for the hydraulic system. The former is fulfilled by Integrated Robust Optimal Design (IROD) proposed in [1, 22] with the latter being the Robust Feedback Linearization (RFL) controller presented in this thesis. The RFL controller is made robust with respect to bulk modulus uncertainties.

1.3 Combine Harvester Header Height Control

The demand for increased productivity in agricultural continues to grow with world population growth. The projected world population in 2050 is over 9 billion people [36], an increase in 30 percent from today, but the number of people working in agriculture continues to drop. In 1900, 41 percent of the workforce was employed in agriculture, by 2000 it was down to only 1.9 percent [37]. One of the most important technological

advances that has made this possible is agricultural equipment. Even though agricultural equipment has allowed new levels of productivity never seen before, it must continue to get more efficient as population grows and labor declines. To become more efficient, yield losses must be minimized, because it is estimated that up to 12 percent of a soybean crop is lost during harvest alone [38] and can be even higher for other types of crops. One important piece of equipment in the harvesting process is the combine harvester, see Fig. 1.1. There are a number of causes for harvest losses, but an estimated 75 percent of the losses occur at the header [39]. One contributing factor to this is missed crop by the header, especially for low lying plants such as soybeans. Automatic header height control attempts to decrease harvest losses, reduce operator fatigue, and protect equipment from damage [40], but has proven to be a challenging control problem. Harvest is a critical time where there is a very small window to achieve maximum yields. For example, soybeans should be harvested once dried to 13 percent, but once below 10 percent damage can occur which increases losses [41]. Weather can make it impossible to get in the field and harvest during a portion of this ideal window, so it becomes even more critical to get crop out as quickly as possible when conditions are right. In terms of the combine harvester, this means speed and productivity can play an important role in decreasing losses. Increased speed makes header height tracking more difficult, so operators instinctively run the header higher off the ground to prevent equipment damage [40]. Thus, the goal becomes increasing speed while also maintaining accurate header height tracking.

Automatic header height control was first seen in the 1950s and 1960s with a number of patents coming out during that time [42–44] and authors recognizing it as a desirable feature [45–47]. Early development involved on-off control [46], and even by the turn of the century on-off control was still considered the standard on state-of-the-art combines [48]. Proportional control was later introduced using PID [49] and LQR [48] control methods. Around the same time, a focus was on the sensors used to track the ground

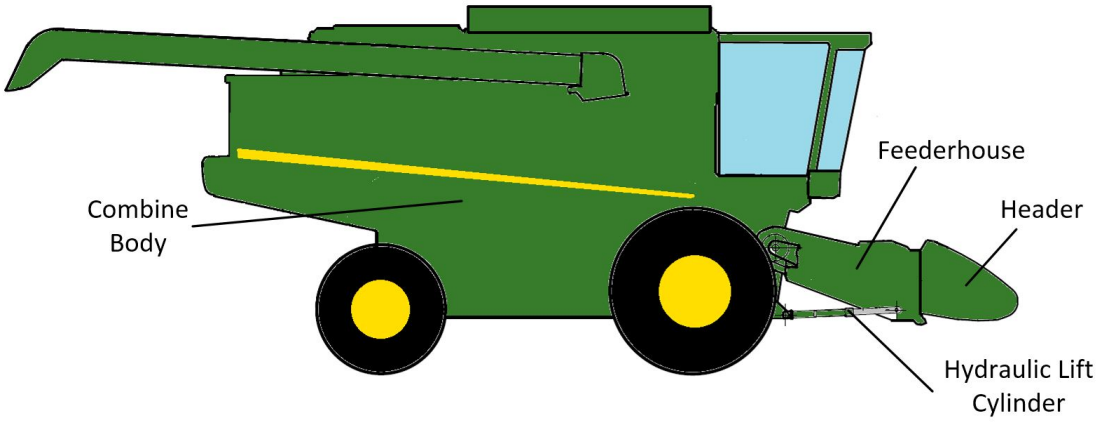

Figure 1.1: Schematic diagram of a typical combine harvester.

profile such as ultrasonic [50] and tactile feedback sensors [51]. More recently, a study was completed analyzing the fundamental limitations of the combine harvester header height control due to the mechanical plant [52]. It suggested that even the best optimal controller still may not be sufficient due to structural limitations. To overcome this, integrated plant and controller design was proposed in [22] and [53]. In doing this, certain mechanical plant parameters are designed concurrently with the controller to achieve a more optimal design than originally possible. In [53], a $\mathcal{H}_\infty$ controller is used, while in [22] a new methodology, IROD, is introduced which is shown to achieve better tracking performance than $\mathcal{H}_\infty$. In both works, the focus is on the mechanical system and the hydraulic dynamics are idealized, such that the hydraulic actuator can provide perfect force. This, of course, is not the case, because a control valve must regulate flow into and out of the cylinder to increase or decrease the pressure, which is directly related to the force output. For this reason, a separate hydraulic controller needs to be designed. This is the control problem that will be addressed in this thesis by designing a robust feedback linearization (RFL) controller for the combine harvester header height hydraulic control system. This controller will be paired with the IROD controller designed in [22]

and tested in simulation over a variety of conditions. The IROD/RFL controller will be compared to the current industry standard, the PID controller, in terms of tracking performance and required control input to the system.

CHAPTER 2. ROBUST FEEDBACK LINEARIZATION

2.1 Non-Affine Feedback Linearization

Standard input-output feedback linearization is limited to nonlinear systems of the form:

$$\begin{aligned} \dot{x} &= f(x) + g(x)u \\ y &= h(x) \end{aligned} \tag{2.1}$$

where, $x \in \Re^n$ is the state vector, $u \in \Re^p$ is the vector of inputs, and $y \in \Re^m$ is the vector of outputs. The process involves finding a coordinate transformation of the nonlinear system such that it is transformed into an equivalent linear system through a change of variables and suitable control input. If the system in Eq. (2.1) is feedback linearizable, a control input can be applied according to the control mapping given in Eq. (2.2), which will render a linear input-output map from a new input ν to the output.

$$u = \alpha(x) + \beta(x)\nu \tag{2.2}$$

Many systems, especially hydraulic systems are not always control affine and rather take the more general form of Eq. (2.3)

$$\begin{aligned} \dot{x} &= f(x,u) \\ y &= h(x) \end{aligned} \tag{2.3}$$

Traditional feedback linearization techniques do not work for these systems, though several design strategies exist. The technique presented in [54, 55] and shown below attempts to turn the original system into an extended control affine system by redefining the states and state equations. To do this, we let a new manipulated input to the system, w be defined as $w = \dot{u}$, and let u be an additional state variable such that the new states, $\bar{x}$ are defined as: $\bar{x} = [x^T \ u^T]^T$. Now the system can be represented as a control affine system:

$$\begin{aligned} \dot{\bar{x}} &= \bar{f}(\bar{x}) + \bar{g}(\bar{x})w \\ y &= h(\bar{x}) \end{aligned} \tag{2.4}$$

where:

$$\bar{x} = \begin{bmatrix} x \\ u \end{bmatrix}, \qquad \bar{f}(\bar{x}) = \begin{bmatrix} f(x,u) \\ 0 \end{bmatrix}, \qquad \bar{g}(\bar{x}) = \begin{bmatrix} 0 \\ 1 \end{bmatrix}, \tag{2.5}$$

From here the standard input-output linearization design procedure can be used with the extended system. Differentiating the output, y, with respect to time to yields:

$$\dot{y} = \frac{dh(\bar{x})}{dt} = \frac{dh(\bar{x})}{d\bar{x}}\frac{d\bar{x}}{dt} = \frac{dh(\bar{x})}{d\bar{x}}[\bar{f}(\bar{x}) + \bar{g}(\bar{x})w] = L_{\bar{f}}h(\bar{x}) + L_{\bar{g}}h(\bar{x})w \tag{2.6}$$

where, $L_{\bar{f}}h(\bar{x}) = \frac{dh(\bar{x})}{d\bar{x}}\bar{f}(\bar{x})$, is called the *Lie Derivative* of h with respect to $\bar{f}$, and likewise, $L_{\bar{g}}h(\bar{x}) = \frac{dh(\bar{x})}{d\bar{x}}\bar{g}(\bar{x})$ is called the *Lie Derivative* of h with respect to $\bar{g}$. If $L_{\bar{g}}h(\bar{x}) = 0$, then

the output rate of change, $\dot{y}$, is not dependent on input, w, and cannot be controlled. Taking time derivative again:

$$\ddot{y} = \frac{d(L_{\bar{f}}h(\bar{x}))}{d\bar{x}}[\bar{f}(\bar{x}) + \bar{g}(\bar{x})w] = L_{\bar{f}}^2 h(\bar{x}) + L_{\bar{g}}L_{\bar{f}}h(\bar{x})w \tag{2.7}$$

If $L_{\bar{g}}L_{\bar{f}}h(\bar{x})$ is still zero, higher derivatives are taken such that:

$$y^{(r)} = L_{\bar{f}}^r h(\bar{x}) + L_{\bar{g}}L_{\bar{f}}^{r-1}h(\bar{x})w \tag{2.8}$$

until $L_{\bar{g}}L_{\bar{f}}^{r-1}h(\bar{x}) \neq 0$. Note that because of the integrator acting on the input, the relative degree of the extended system is $r = \rho + 1$, where ρ is the relative degree of the original non-affine system. The coordinate transformation comes from the first $(r-1)$ derivatives, which transforms the system from the original $\bar{x}$ coordinate system into a new z coordinate system.

$$z = \begin{bmatrix} z_1(\bar{x}) \\ z_2(\bar{x}) \\ \vdots \\ z_r(\bar{x}) \end{bmatrix} = \begin{bmatrix} y \\ \dot{y} \\ \vdots \\ y^{(r-1)} \end{bmatrix} = \begin{bmatrix} h(\bar{x}) \\ L_{\bar{f}}h(\bar{x}) \\ \vdots \\ L_{\bar{f}}^{r-1}h(\bar{x}) \end{bmatrix} \tag{2.9}$$

The resulting linearized system, shown in Eq. (2.10) is a cascade of r integrators and the transformed input, ν, which we define according to Eq. (2.11).

$$\begin{bmatrix} \dot{z_1}(\bar{x}) \\ \dot{z_2}(\bar{x}) \\ \vdots \\ \dot{z_r}(\bar{x}) \end{bmatrix} = \begin{bmatrix} z_2(\bar{x}) \\ z_3(\bar{x}) \\ \vdots \\ \nu \end{bmatrix} \tag{2.10}$$

$$\nu = y^{(r)} = L_{\bar{f}}^{r} h(\bar{x}) + L_{\bar{g}} L_{\bar{f}}^{r-1} h(\bar{x}) w \tag{2.11}$$

If we solve for w in Eq. (2.11), then the linearizing feedback control mapping can be calculated as:

$$w = \frac{\nu - L_{\bar{f}}{}^{r} h(\bar{x})}{L_{\bar{g}} L_{\bar{f}}{}^{r-1} h(\bar{x})} \tag{2.12}$$

or putting it in terms of the original input:

$$\dot{u} = \frac{\nu - L_{\bar{f}}{}^{r} h(\bar{x})}{L_{\bar{g}} L_{\bar{f}}{}^{r-1} h(\bar{x})} \tag{2.13}$$

where ν can be chosen according to Eq. (2.14) with reference signal R.

$$\nu = K(R - z) = K_1(R - y) + K_2 \frac{d(R-y)}{dt} + \cdots + K_r \frac{d^{r-1}(R-y)}{dt^{r-1}} \tag{2.14}$$

The gains $K_1, K_2, ...K_r$ are chosen to stabilize the system. Theoretically higher gains will result in better tracking performance, but too high of gains can result in high frequency oscillations or chattering, especially with the higher derivative terms and could lead to instability. The block diagram for the feedback linearization control structure is shown in Fig. 2.1.

2.2 Robust Control Design

Feedback linearization controllers by nature lack robustness, because the calculated control input from Eq. (2.13), is highly dependent on accurate knowledge of the system.

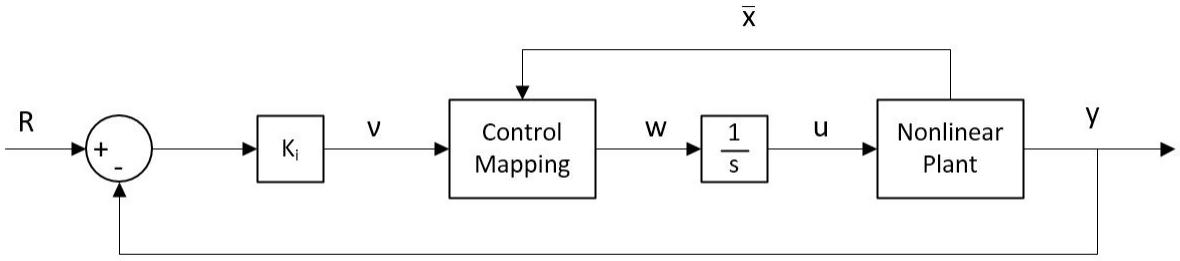

Figure 2.1: Feedback linearization control structure for a general control non-affine system.

This can become problematic if there are parameters in the system equations which are uncertain. This could be due to difficult to measure parameters, constantly changing parameters, or deterioration due to normal wear and tear. To account for this, the nominal feedback linearization controller will be made more robust to a select uncertain parameter. This is done by augmenting the system with sensitivity dynamics and adjusting the control input to minimize this sensitivity.

2.2.1 Introduction to Sensitivity Dynamics

Parametric sensitivity describes how a system changes due to variations in a given parameter. For a continuous plant model, the parametric sensitivity is calculated by differentiating the dynamical state equations with respect to the uncertain parameter or parameters that are subject to change. Ideally, a system will have a very small change in performance for a given change in an uncertain parameter.

Consider a generic linear system in Eq. (2.15) where $x \in \Re^n$ is the state vector, $u \in \Re^p$ is the vector of inputs, $y \in \Re^m$ is the vector of outputs, and $b \in \Re$ is an unknown parameter. This technique can also be extended to a system where $b \in \Re^k$ is a vector of multiple unknown parameters, but it will be assumed to be a scalar in this study.

$$\begin{aligned} \dot{x} &= f(x,b) + g(x,b)u \\ y &= h(x,b) \end{aligned} \tag{2.15}$$

The sensitivity dynamics of Eq. (2.15) can be calculated as:

$$\begin{aligned} \frac{d\dot{x}}{db} &= \frac{df}{db} + \frac{dg}{db}u = \frac{\partial f}{\partial b} + \frac{\partial f}{\partial x}\frac{\partial x}{\partial b} + \frac{\partial g}{\partial b} + \frac{\partial g}{\partial x}\frac{\partial x}{\partial b}u \\ \frac{dy}{db} &= \frac{dh}{db} = \frac{\partial h}{\partial b} + \frac{\partial h}{\partial x}\frac{\partial x}{\partial b} \end{aligned} \tag{2.16}$$

which, can be written more simply as:

$$\begin{aligned} \dot{x}_b(x, x_b, u, b) &= f_b(x, x_b, b) + g_b(x, x_b, b)u \\ y_b(x, x_b, b) &= h_b(x, x_b, b) \end{aligned} \tag{2.17}$$

where $x_b \in \Re^n$ is the sensitivity state vector, y_b is the output sensitivity, and elsewhere the subscript b represents a full derivative with respect to the unknown parameter b, mathematically written as:

$$(.)_b = \frac{\partial(.)}{\partial b} + \frac{\partial(.)}{\partial x}x_b \tag{2.18}$$

It is implied that the control input, u, is independent of the unknown parameter, b. In the case of feedback control, this does not hold true, because the output is used for the control input calculation, so u is indirectly parameter dependent. Because of this, the derivative of u with respect to b must also be considered. Due to the chain rule, the sensitivity dynamics become:

$$\begin{aligned} \dot{x}_b(x, x_b, u, u_b, b) &= f_b(x, x_b, b) + g_b(x, x_b, b)u + g(x, b)u_b \\ y_b(x, x_b, b) &= h_b(x, x_b, b) \end{aligned} \tag{2.19}$$

where $u_b = \frac{du}{db}$ is the variation in control input to be designed in the next section.

2.2.2 Control design

Returning to the feedback linearization design of the system in Eq. (2.4), the sensitivity dynamics can be augmented with the system equations as shown in Eq. (2.20). Here, the $(\bar{\cdot})$ notation has been left out for simplicity in this section, but it can be applied to the extended affine system in Eq. (2.4) with $x = \bar{x}$, $f = \bar{f}$, and $g = \bar{g}$.

$$\begin{aligned} \dot{x} &= f(x, b) + g(x, b)w \\ \dot{x}_b &= f_b(x, x_b, b) + g_b(x, x_b, b)w + g(x, b)w_b \\ y &= h(x, b) \\ y_b &= h_b(x, x_b, b) \end{aligned} \tag{2.20}$$

The augmented state vector becomes $\mathcal{X} = [x^T, x_b^T]^T$, and the system has two inputs, w and w_b, and two outputs, y and y_b. The input w, is calculated from the nominal feedback linearization control law in Eq. (2.12) and the input w_b, is the variation in the control input to be designed. The objective of robust feedback control input, w_b is to minimize the sensitivity and thus, make the system more robust. The stability and feedback linearization for the sensitivity augmented system was first presented in [1] by way of proving three theorems. It is shown that for the system in Eq. (2.20) the sensitivity of the transformed input, ν can be calculated as:

$$\nu_b = \frac{d}{db}L_f^r h + \frac{d}{db}(L_g L_f^{r-1} h \cdot w) \tag{2.21}$$

Applying the chain rule to the second term in Eq. (2.21), it becomes:

$$\nu_b = L_f^r h_b(x, x_b) + L_g L_f^{r-1} h_b(x, x_b) w + L_g L_f^{r-1} h(x) w_b \tag{2.22}$$

where the subscript b follows the same convention as shown in Eq. (2.18). Solving for w_b in Eq. (2.22) the adjustment to the feedback linearizing control becomes:

$$w_b = \dot{u}_b = \frac{\nu_b - L_f^r h_b(x, x_b) - L_g L_f^{r-1} h_b(x, x_b) w}{L_g {L_f}^{r-1} h(x)} \tag{2.23}$$

where ν_b can be chosen according to Eq. (2.24) with reference signal R_b.

$$\nu_b = K_{b_1}(R_b - y_b) + K_{b_2}\frac{d(R_b - y_b)}{dt} + \cdots + K_{b_r}\frac{d^{r-1}(R_b - y_b)}{dt^{r-1}} \tag{2.24}$$

Because the desired sensitivity is 0, the sensitivity reference signal is $R_b = 0$. Applying this to Eq. (2.24), it becomes:

$$\nu_b = -K_{b_1} y_b - K_{b_2}\frac{dy_b}{dt} - \cdots - K_{b_r}\frac{d^{r-1} y_b}{dt^{r-1}} \tag{2.25}$$

The gains $K_{b_1}, K_{b_2}, ...K_{b_r}$ are chosen to stabilize the sensitivity dynamics. As with the nominal system, theoretically higher gains will result in better tracking performance, but too high of gains can result in high frequency oscillations or chattering, especially with the higher derivatives. The block diagram for the robust feedback linearization control system is shown in Fig 2.2.

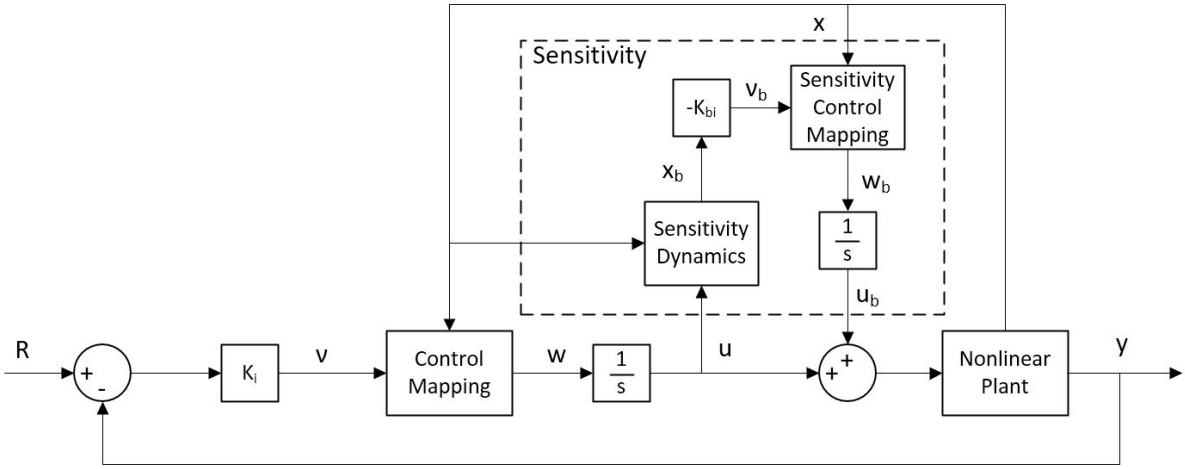

Figure 2.2: Robust feedback linearization control structure for a general control non-affine system.

CHAPTER 3. DESIGN PROCESS OF A GENERAL HYDRAULIC SYSTEM

The robust feedback linearization control design process is ideally suited for hydraulic systems, specifically the control of hydraulic actuators. Fluid power (hydraulics) is used extensively in the mobile equipment industry and is often used in conjunction with electronics and software for control of the vehicle. This requires detailed knowledge of both the hydraulic system and the multi-body dynamics of the mechanical system. In this study two separate controllers are used to control the machine function. Robust feedback linearization is used to design the hydraulic system controller, and the integrated robust optimal design methodology is used to design the mechanical system controller, which will be introduced in the next section. This chapter will explain the general design methodology for a hydraulically controlled, multi-body machine.

3.1 Integrated Robust Optimal Design (IROD) Controller

This section provides a brief introduction to the methodology for integrated robust optimal design (IROD), originally presented in [1, 22]. This methodology combines traditional sensitivity theory with relatively new advancements in Bilinear Matrix Inequality (BMI) constrained optimization problems, which provides the least conservative approach for robust control synthesis. By expressing the robustness in the form of sensitivity, the synthesis process can be automated and allows the extension to integrated design, where structural parameters can be designed concurrently with a controller.

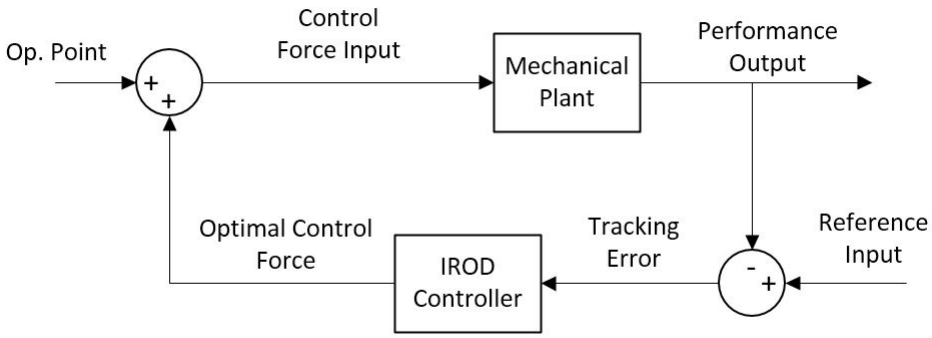

Figure 3.1: Closed loop system with IROD controller for a multi-body mechanical system.

The IROD methodology has been demonstrated in two application examples with the general control structure as shown in Fig. 3.1. Here, there was no hydraulic system involved, so the optimal control forces calculated from the IROD controller were added to the operating point and fed directly to the mechanical plant. It was is compared to the current state of the art sequential design methodology, $\mathcal{H}_\infty$, which was set up in the same control structure. The results showed that IROD provides a viable alternative for robust controller synthesis and can offer better tracking, robustness, and control power than the $\mathcal{H}_\infty$ design method.

3.2 Overall Design Procedure

The overall design process for a general hydraulically controlled mechanical system is given in Fig. 3.2. The first row involves the mechanical system, while the second row involves the hydraulic system. The design process of each of these is completely independent of the other. For example, the IROD controller design is only dependent on the mechanical system plant parameters and likewise for the robust feedback linearization controller and the hydraulic system. The final step links the mechanical and hydraulic system plants, along with the IROD and robust feedback linearization controller, which includes sensitivity dynamics, into a closed loop system for simulation.

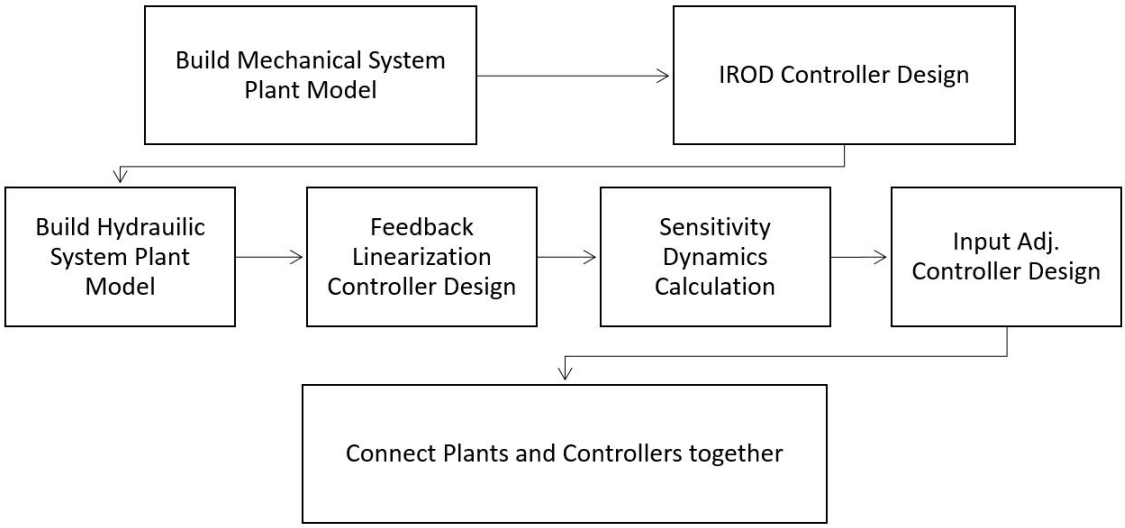

Figure 3.2: Process Flowchart for the design process of a general hydraulically controlled mechanical system.

Figure 3.3 shows a high-level view of how these systems are connected. The overall layout is the same as the IROD control structure, with the addition of the hydraulic system. The desired control force, instead of going directly to the mechanical plant, is used as the reference signal for the feedback linearization controller. The nominal feedback linearization output, u, and the states, x, are used to calculate the sensitivity dynamics and adjust the control input to minimize the sensitivity before being fed into the hydraulic plant. Physically, this control input is the current to the hydraulic control valve, which regulates flow to the hydraulic actuator. The actual hydraulic force from the hydraulic actuator is then fed into the mechanical plant where the performance output is measured. A more detailed control structure is shown in Fig. 3.4.

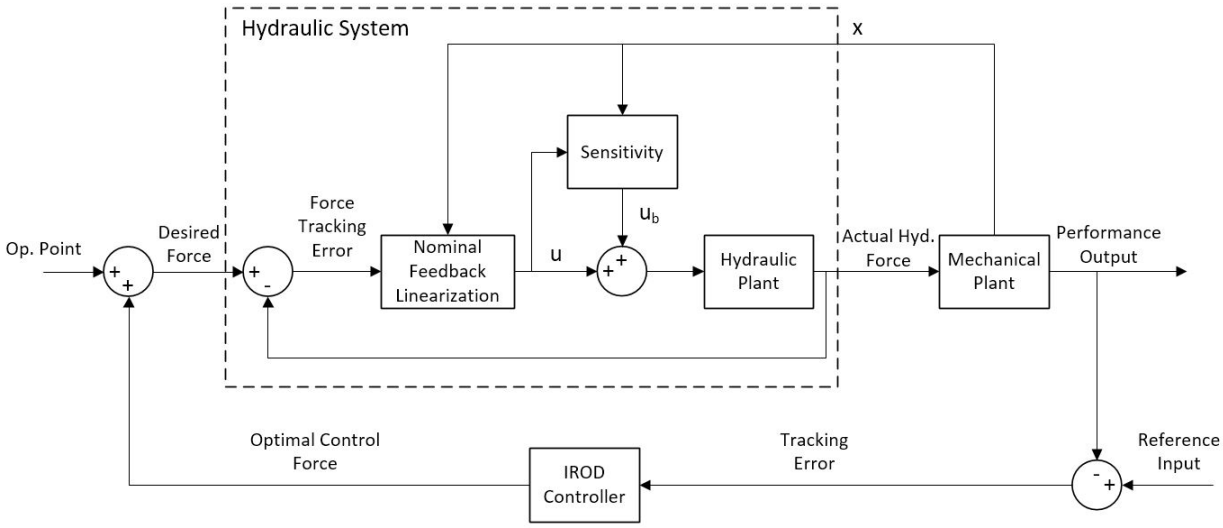

Figure 3.3: High-level control structure of hydraulically controlled mechanical system using IROD and robust feedback linearization controllers.

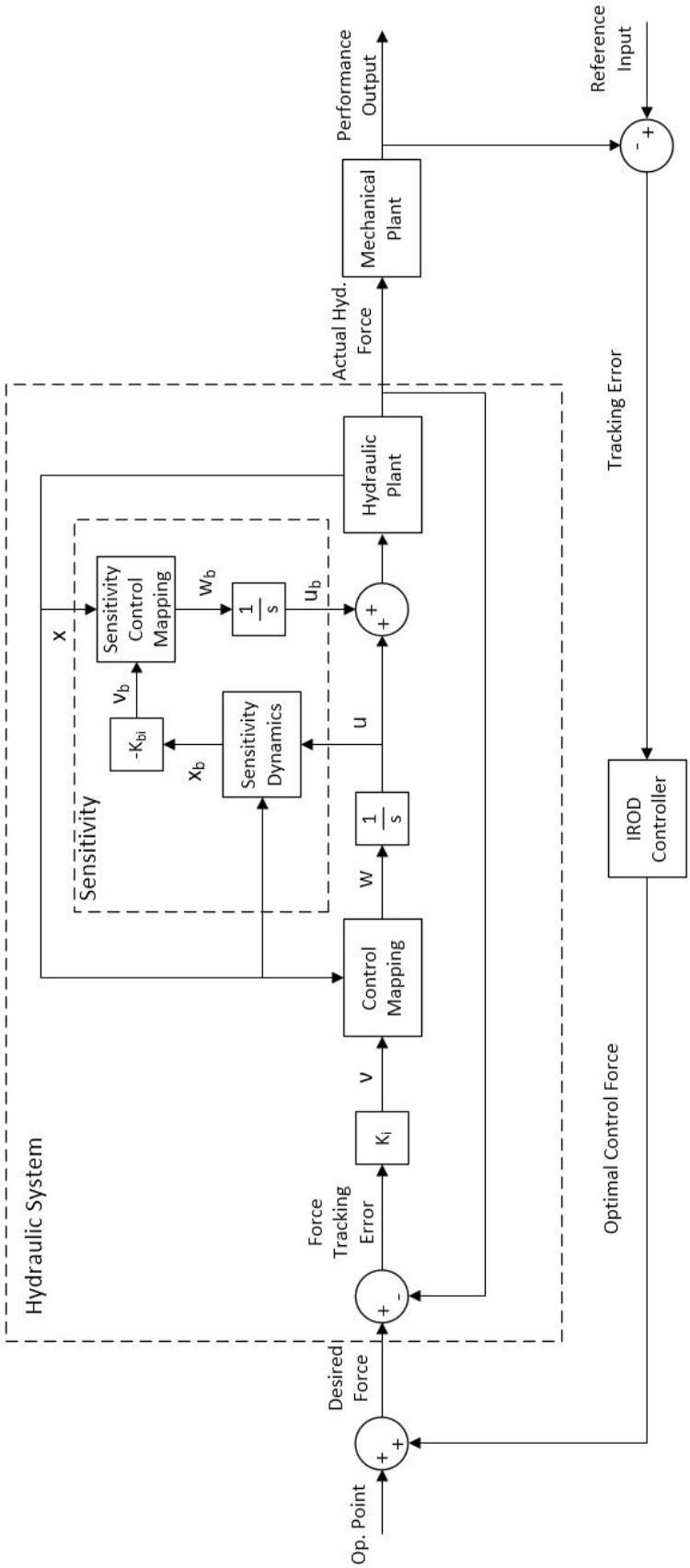

Figure 3.4: Detailed control structure of hydraulically controlled mechanical system using IROD and robust feedback linearization controllers.

CHAPTER 4. APPLICATION TO COMBINE HARVESTER

The design methodology proposed in the previous chapter is used to design a controller for automatic header height control of the combine harvester. The schematic for a typical combine harvester is shown in Figure 4.1. The objective is to improve tracking performance of the header to the terrain as the combine is moving forward, while also optimizing control inputs and making it robust to uncertain parameters. This would allow for higher productivity due to fewer harvest losses and increased harvesting speed. The controller designed for the mechanical system is based on the IROD methodology presented in [1, 22], while the hydraulic controller is designed using the robust feedback linearization presented in Chapter 2. The controlled system is then tested over various travel speeds and terrain conditions to verify the performance and is compared to the commonly used PID design.

4.1 Plant Modeling

The combine harvester was modeled and simulated using the MATLAB SimScape environment. The model parameters were based off of a combine harvester produced by John Deere. The plant was simplified to include only the components relevant to the header height control while still capturing the critical machine dynamics.

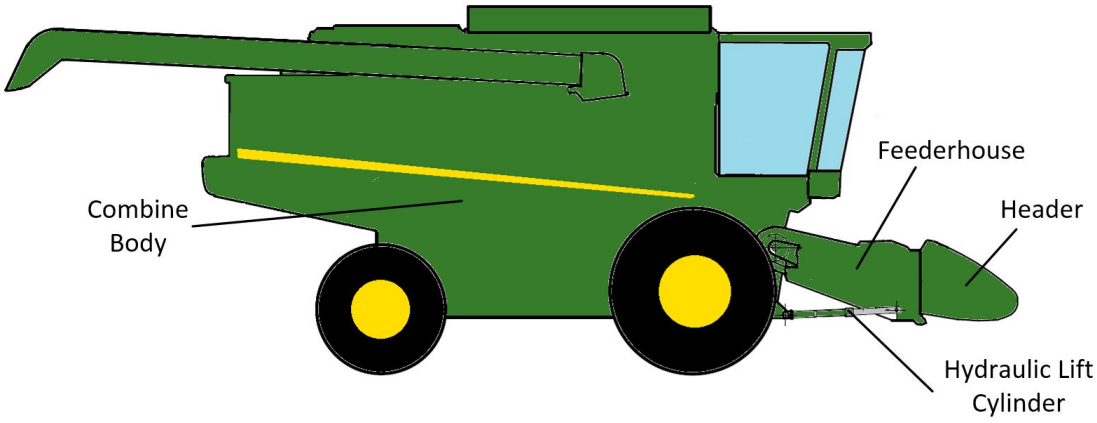

Figure 4.1: Schematic diagram of a typical combine harvester.

4.1.1 Mechanical plant model

The mechanical system was modeled using the first generation SimMechanics package in MATLAB. The model includes a 2-dimensional representation of the combine body, header lift mechanism, and tire dynamics. The complete model is shown in Fig. 4.2.

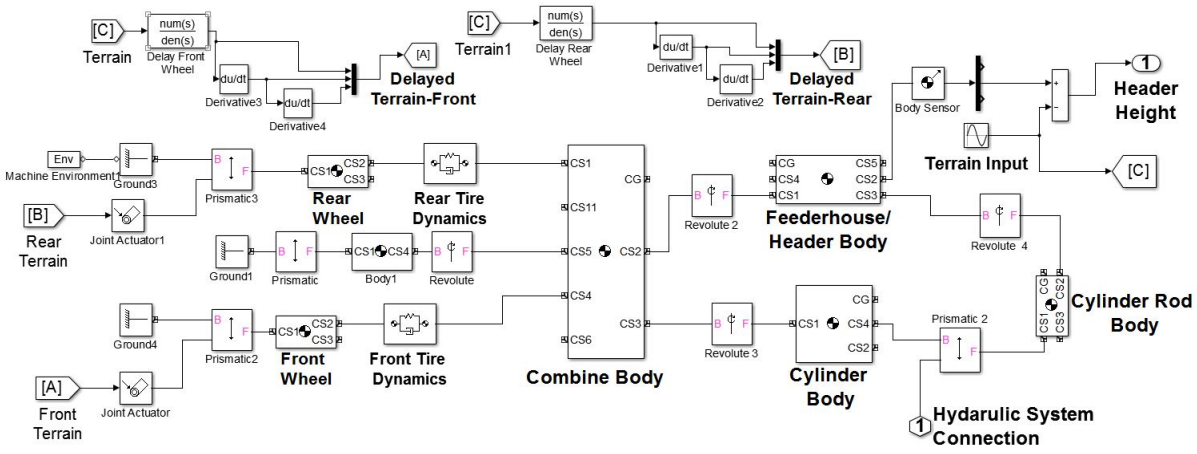

Figure 4.2: Mechanical plant model of combine harvester in SimMechanics

The *Combine Body* block is a general body block that includes the estimated mass and moment of inertia of all components on the combine harvester, besides the bodies specified individually in the model. It also assumes the machine is loaded to approximately half of its grain capacity. All of the body specifications are given in Table 4.1. The terrain input is modeled as a sine wave with varying amplitude and frequency. Because the height sensor is in the header, there is a delay between the input signal from the sensor and the reaction at the front and rear tires. Since these distances are constant, the delay can be calculated as a function of the combine harvester velocity. This delay is modeled in MATLAB using the first order Pade approximation to get a transfer function equivalent to the delays.

Table 4.1: Mechanical plant parameters for the combine harvester SimMechanics model.

Component	**Mass** (kg)	**Inertia** $(kg - m^2)$
Combine Body	20,200	61,310
Feederhouse/Header	3,800	5060
Cylinder Body	15	1
Cylinder Rod	30	2
Front Wheel	440	301
Rear Wheel	176	64

The structural design variable chosen for integrated design is the pin joint location, where the hydraulic cylinder rod connects to the feederhouse body. The IROD methodology is used to synthesize a controller and optimize the structural design variable concurrently such that sensitivity, tracking error, and control power are minimized. The nominal distance between the pin joint locations is 1.51m, but the proposed change is to move it 6.36cm closer as shown in Fig. 4.3. The full IROD synthesis process is detailed in [1, 22].

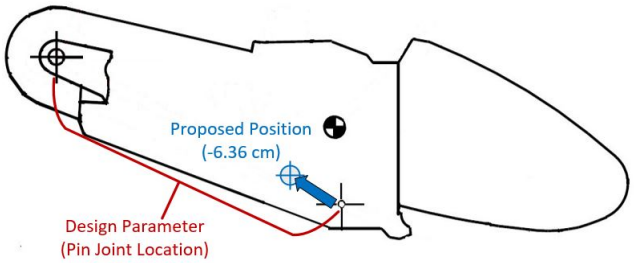

Figure 4.3: Proposed design parameter change in combine harvester feederhouse/header from the IROD controller synthesis.

4.1.2 Hydraulic plant model

The header height is actuated by two single-acting hydraulic cylinders, which are controlled by two proportional 2-way poppet valves. One valve controls flow into the cylinders from a high pressure pump line, while the other controls flow leaving the cylinders, which returns to the tank or reservoir. The header height hydraulic schematic is shown in Figure 4.4.

Since this study focuses on 2-dimensional planar mechanics, this diagram can be simplified by using one single-acting cylinder, with twice the piston area. Additionally, the prime mover and pressure compensated pump can be idealized by using a constant pressure source. Finally, the check valves were replaced with closed positions in the poppet valves. This is justified on the high pressure side because there is an external check valve opposite to the valve, essentially acting as closed position. On the reservoir side, it is assumed that the reservoir pressure is zero, so there would never be any pressure to open the check valve. The simplified diagram was modeled using the SimHydraulics package in MATLAB, which is shown in Fig. 4.5. The poppet valves are modeled as 2-way directional valves using pressure-flow tables. The selection and development of the valve equations are explained in the next section. The remainder of the hydraulic parameters used in the plant model are given in Table 4.2.

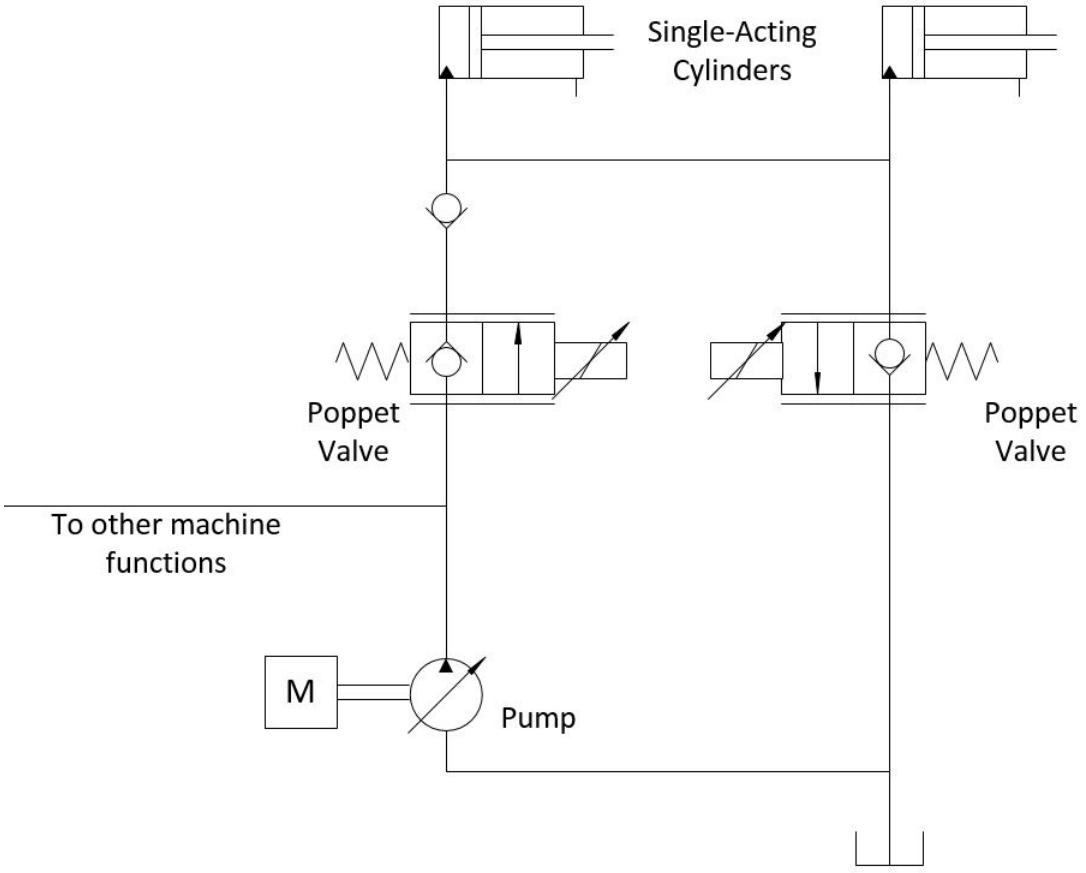

Figure 4.4: Hydraulic schematic of header height control in a combine harvester.

Table 4.2: Hydraulic system parameters for the combine harvester SimHydraulics model.

Parameter	**Symbol**	**Value**	**Unit**
Piston Area	A	0.0127	m^2
Piston Stroke	L	0.587	m
Dead Volume	V_0	5×10^{-5}	m^3
Pump Pressure	P_s	2.14×10^7	Pa
Tank Pressure	P_t	0	Pa
Fluid Density	ρ	867	Kg/m^3
Fluid Bulk Modulus	β	1.45×10^9	Pa

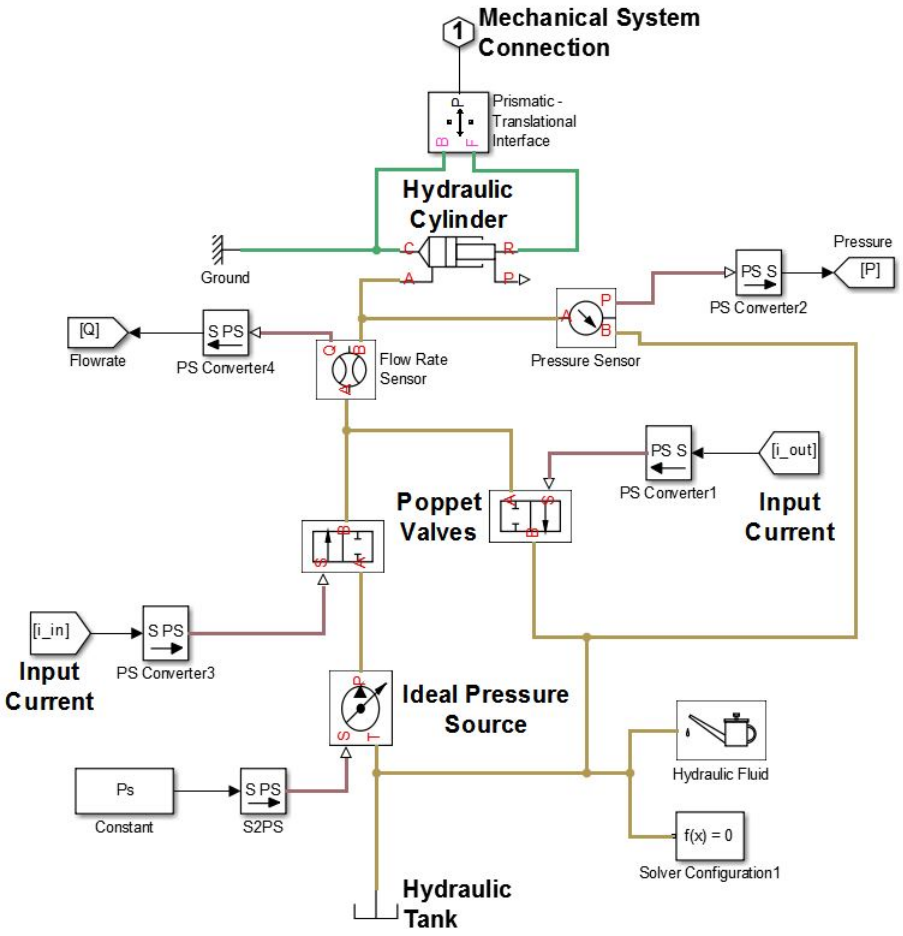

Figure 4.5: Hydraulic plant model of combine harvester's header lift system in SimHydraulics

4.2 Dynamic Equation Development

4.2.1 Hydraulic equations of motion

The hydraulic equations of motion will be developed for the system given in Fig. 4.6. The effects of leakage, resistance in the connections, and thermal changes will be neglected.

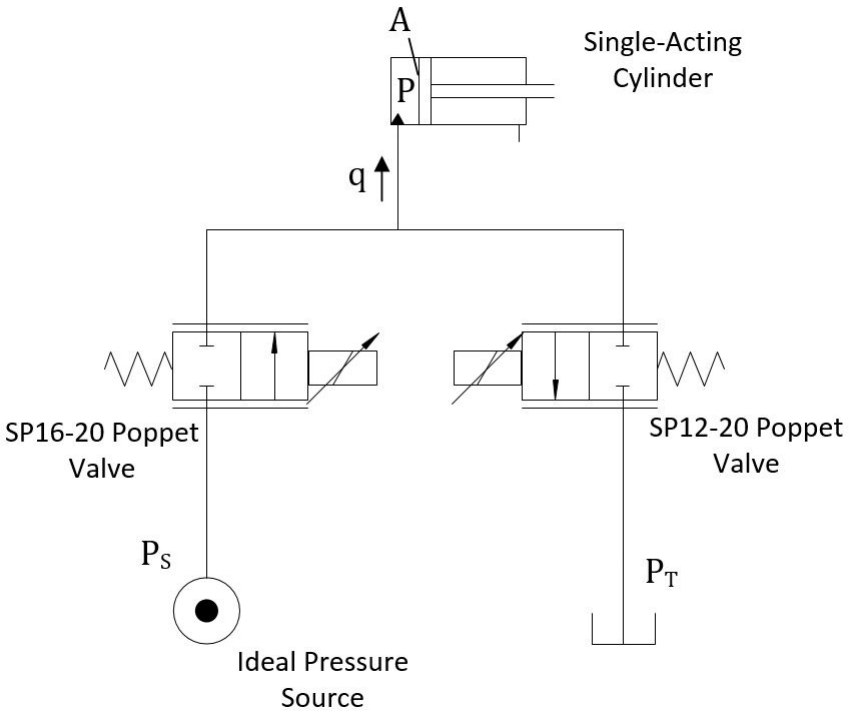

Figure 4.6: Simplified hydraulic schematic for 2-D planar header motion of the combine harvester.

The poppet valves chosen are the HydraForce SP16-20 and SP12-20 for controlling flow in and out of the hydraulic cylinder, respectively. These valves are solenoid-operated, two-way, normally closed cartridge valves. The flow is a function of the current applied to the coil as well as the pressure drop across the valve. Performance flow curves for the SP16-20 and SP12-20 are shown in Fig. 4.8 and can be found on the HydraForce website [56].

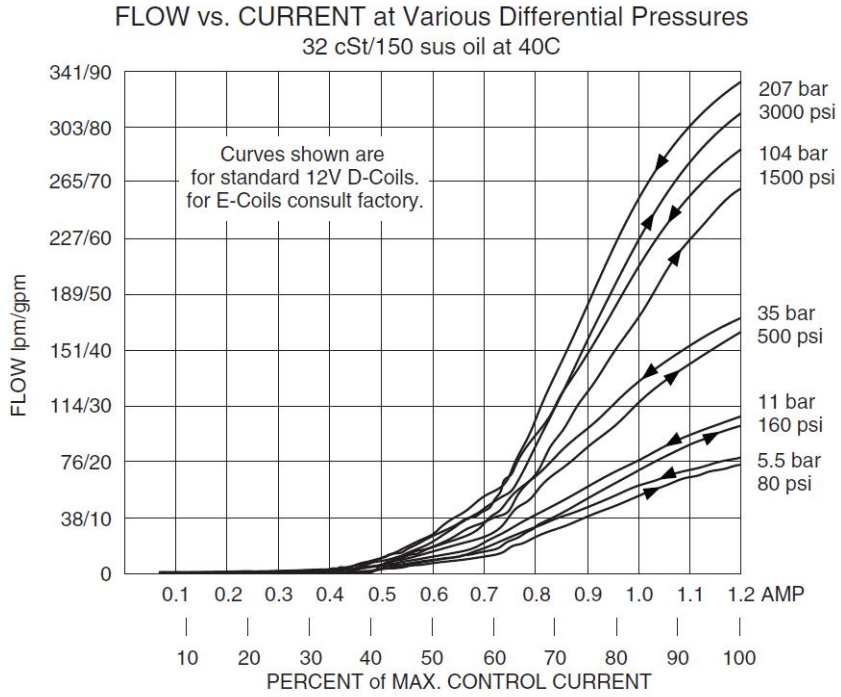

(a) Hydra Force SP16-20

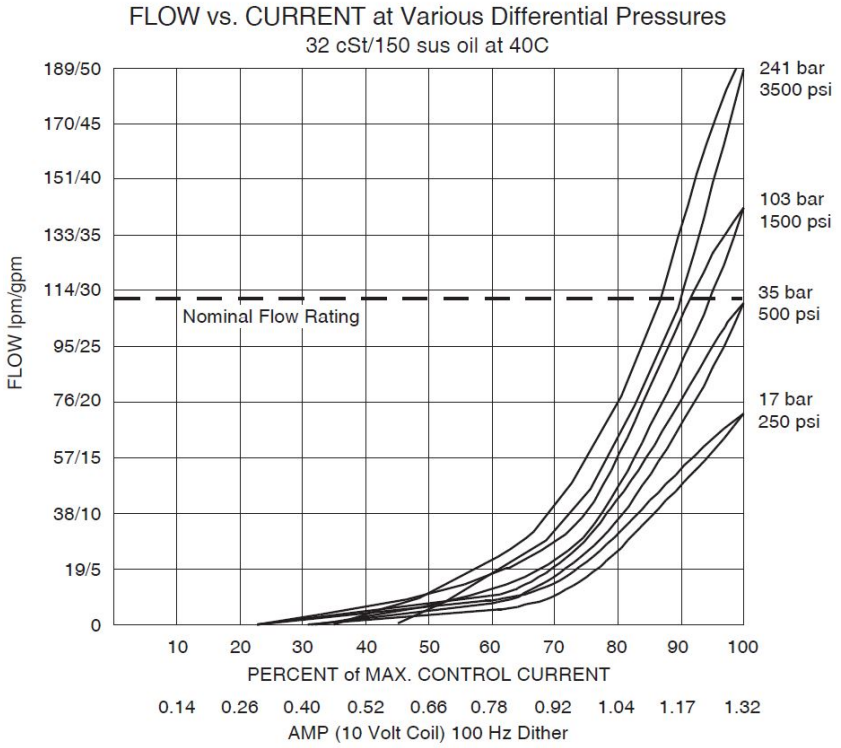

(b) Hydra Force SP12-20

Figure 4.8: Hydra Force poppet valve performance plots showing flow as a function of input current and differential pressure.

A multivariable model can be calibrated for each of these valves using MATLAB's Curve Fitting Toolbox. The performance curve values were tabulated with an n dimensional array for control current, a m dimensional array for differential pressure, and an $m \times n$ dimensional array for the corresponding flow rates. Hysteresis effects were ignored by taking an average flow rate for a given current and pressure. Since dead bands are difficult to model mathematically, only data points above the cracking current were included. Below the cracking current, there was assumed to be no flow, or leakage. The flow-current relationship was modeled using a polynomial function:

$$q = a_1\, i + a_2\, i\, \Delta p + a_3\, i^2 + a_4\, i^2\, \Delta p \tag{4.1}$$

where a_1 to a_4 are constants determined by the Curve Fitting Toolbox for each valve. Additionally, weights were used to eliminate any negative flow rates at low current and maintain $\frac{dq}{d\Delta p} > 0$ (i.e higher flow at higher differential pressure). The constants for the SP16-20 and SP12-20 valve equations are given in Table 4.3 in standard SI units for flow and pressure . Plotting the equations over the same current and pressure ranges as the supplier performance curves gives the plots shown in Fig. 4.10. The flow equations track the tabulated data very will with an R-squared value of 0.981 and 0.971 for the SP16-20 and SP12-20 valves, respectively.

Table 4.3: Poppet valve polynomial equation constants

Constant	**SP16-20**	**SP12-20**
a_1	1.905×10^{-3}	1.990×10^{-5}
a_2	1.948×10^{-11}	2.293×10^{-12}
a_3	3.417×10^{-3}	3.619×10^{-3}
a_4	3.519×10^{-10}	1.359×10^{-10}

These equations hold for pressure ranges of 35-207 bar and 35-241 bar for the SP16-20 and the SP16-12 valves, respectively. While the fit could be expanded for a larger pressure range, it comes at the expense of worse tracking. This range was chosen based on the expected operating range of the header height hydraulic cylinder. Other equation forms could also be used with additional terms if higher accuracy is desired. Because a standard valve equation contains a term with the square root of the pressure, using this in Eq. (4.1) may also improve the fit. The equation used was simply modified from a standard polynomial equation with only terms containing i included, such that the flow is zero when control current is zero (cracking current).

Equation (4.2) describes the motion of a single acting hydraulic actuator, where X is the cylinder position, V is the cylinder velocity, and q is the flow rate into the cylinder. The remaining variables follow the same notation given in Table 4.2.

$$\dot{P} = \frac{\beta}{A\,X + V_0}\,(q - A\,V) \tag{4.2}$$

The hydraulic equations of motion can be found by combining the poppet valve equation, Eq. (4.1), and the single-acting cylinder equation, Eq. (4.2). There will be two different cases when combing the equations: raising and lowering the header, which is when fluid is entering the cylinder by means of the SP16-20 valve or when fluid is exiting by means of the SP12-20 valve, respectively. When raising, the pressure drop across the poppet valve will be: $\Delta p = P_s - P$. Whereas, when lowering, the pressure drop will be: $\Delta p = P - P_t$ or $\Delta p = P$ if the hydraulic reservoir pressure is zero. Additionally, for this case the flow rate will be negative in Eq. (4.2). A single input current i will be used for both cases; positive values will represent raising the header, while negative values will be lowering. Because the poppet valve equations in Eq. (4.1) assume a positive input, the notation, $\bar{i}$ will be used in the lowering equations where $\bar{i} = -i$. Additionally, since the constants for the flow equations differ for the two poppet valves, a_1 - a_4 will be replaced

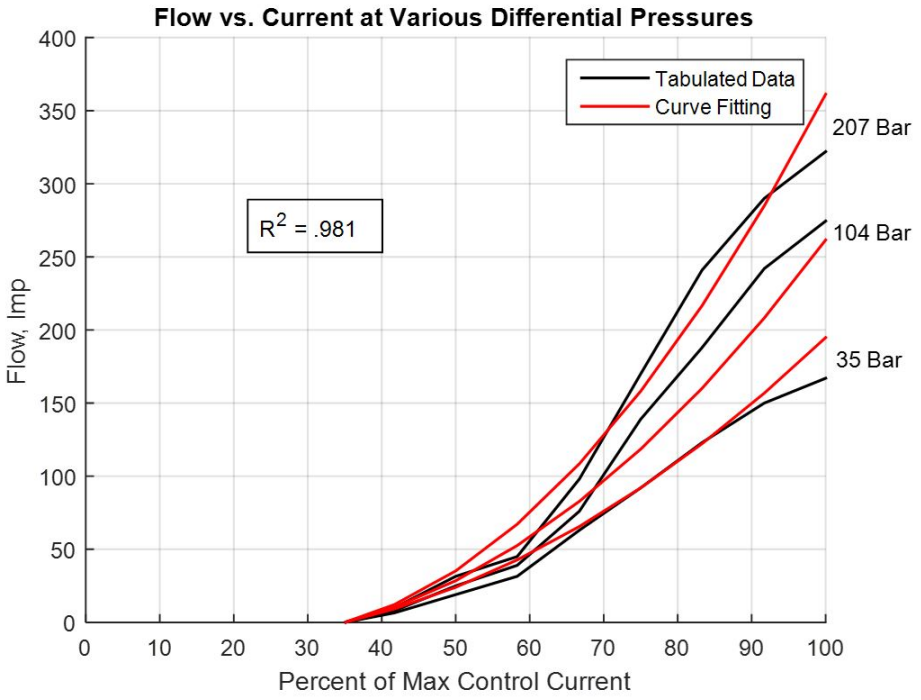

(a) Hydra Force SP16-20

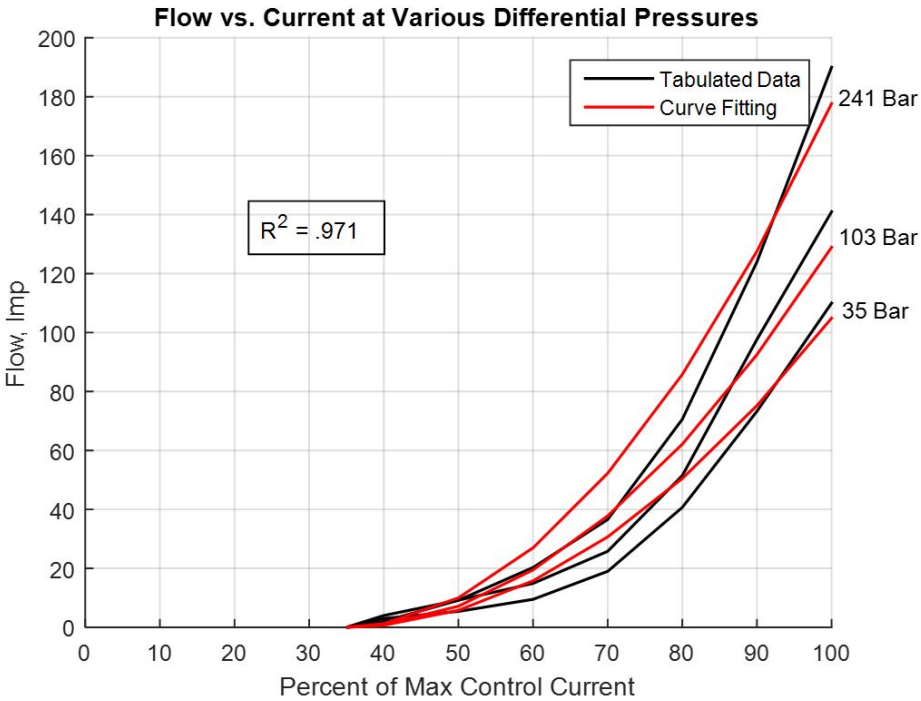

(b) Hydra Force SP12-20

Figure 4.10: Estimated performance plots using a custom equation fit of poppet valve tabulated data for flow rate as a function of input current and differential pressure.

with b_1 - b_4 of the lowering case, where b_1 - b_4 represent the constants for the SP12-20 valve. The resulting equations are shown in Eq. (4.3) and Eq. (4.4).

$$i \geq 0 : \tag{4.3}$$
$$\dot{P} = \frac{\beta}{A\,X + V_0}\left(a_1\,i + a_2\,i\,(P_s - P) + a_3\,i^2 + a_4\,i^2\,(P_s - P) - A\,V\right)$$

$$i < 0 : \tag{4.4}$$
$$\dot{P} = \frac{-\beta}{(A\,X + V_0)}\left(b_1\,\bar{i} + b_2\,\bar{i}\,P + b_3\,\bar{i}^2 + b_4\,\bar{i}^2\,P + A\,V\right)$$

The output of the hydraulic system is the force provided by the hydraulic cylinder, which is given by the following equation:

$$F = P\,A \tag{4.5}$$

4.2.2 State-space model

From the hydraulic equations of motion, we can form a state space model for the combine harvester header height hydraulic system according to Eq. (4.6), where $x \in \Re^n$ is the state vector, $i \in \Re$ is the input current, and $F \in \Re$ is the force output.

$$\begin{aligned} \dot{x} &= f(x, i) \\ F &= h(x) \end{aligned} \tag{4.6}$$

Let the states be defined as: $x = [X\ V\ P]^T$, namely cylinder position, cylinder velocity, and cylinder pressure, respectively. Then the state space system is given by:

$$\begin{bmatrix} \dot{X} \\ \dot{V} \\ \dot{P} \end{bmatrix} = \begin{bmatrix} V \\ \frac{1}{m}\left(P\,A - F_{load}\right) \\ Eq.\ (4.3)\ or\ Eq.\ (4.4) \end{bmatrix}$$
$$\begin{bmatrix} F \end{bmatrix} = \begin{bmatrix} P\,A \end{bmatrix} \tag{4.7}$$

Here, $\dot{V}$ is the acceleration of the cylinder, which can be found from Newton's second law of motion: $\Sigma F = ma$. This will be a function of the mass, m, and the external load on the hydraulic cylinder, F_{load}, which depends on the multi-body dynamics of the mechanical system.

4.3 Controller Design

4.3.1 Nominal Feedback Linearization

The next step is to design the nominal feedback linearizing controller for the hydraulic system given in Eq. (4.7). Because the equations are control non-affine, we will apply the input-output feedback linearization technique presented in Chapter 2. First, the system will be made control affine by redefining the states and input. Let $w = \frac{di}{dt}$, where w is the new input to the system, and let i be an additional state variable. That is, $\bar{x} = [x^T\ i]^T$, where $\bar{x} \in \Re^{n+1}$ is the extended state vector. Now the system can be represented as a control affine system given below:

$$\begin{bmatrix} \dot{X} \\ \dot{V} \\ \dot{P} \\ \dot{i} \end{bmatrix} = \begin{bmatrix} V \\ \frac{1}{m}\left(P\,A - F_{load}\right) \\ Eq.\ (4.3)\ or\ Eq.\ (4.4) \\ 0 \end{bmatrix} + \begin{bmatrix} 0 \\ 0 \\ 0 \\ 1 \end{bmatrix} w$$

$$\begin{bmatrix} F \end{bmatrix} = \begin{bmatrix} P\,A \end{bmatrix} \tag{4.8}$$

The system in Eq. (4.8) has the same form as:

$$\begin{aligned} \dot{\bar{x}} &= \bar{f}(\bar{x}) + \bar{g}(\bar{x})w \\ y &= h(\bar{x}) \end{aligned} \tag{4.9}$$

Calculating the Lie derivatives:

$$L_{\bar{f}}h(\bar{x}) = \frac{dh(\bar{x})}{d\bar{x}}\bar{f}(\bar{x}) = \begin{bmatrix} 0 & 0 & A & 0 \end{bmatrix} \begin{bmatrix} V \\ \frac{1}{m}\left(P\,A - F_{load}\right) \\ Eq.\ (4.3)\ or\ Eq.\ (4.4) \\ 0 \end{bmatrix}$$

$i \geq 0$: (4.10)

$$= \frac{\beta\,A}{A\,X + V_0}\left(a_1\,i + a_2\,i\,(P_s - P) + a_3\,i^2 + a_4\,i^2\,(P_s - P) - A\,V\right)$$

$i < 0$: (4.11)

$$= \frac{-\beta\,A}{(A\,X + V_0)}\left(b_1\,\bar{i} + b_2\,\bar{i}\,P + b_3\,\bar{i}^2 + b_4\,\bar{i}^2\,P + A\,V\right)$$

$$L_{\bar{g}}h(\bar{x}) \;=\; \frac{dh(\bar{x})}{d\bar{x}}\bar{g}(\bar{x}) \;=\; \begin{bmatrix} 0 & 0 & A & 0 \end{bmatrix} \begin{bmatrix} 0 \\ 0 \\ 0 \\ 1 \end{bmatrix} \;=\; 0 \tag{4.12}$$

The output rate of change, $\dot{F}$, can be calculated as: $\dot{F} = L_{\bar{f}}h(\bar{x}) + L_{\bar{g}}h(\bar{x})w$. Since $L_{\bar{g}}h(\bar{x}) = 0$, the output is not dependent on input, w, and cannot be controlled. Taking the Lie derivatives again:

$i \geq 0$:

$$\begin{aligned} L_{\bar{f}}^2 h(\bar{x}) =& \frac{dL_{\bar{f}}h(\bar{x})}{d\bar{x}}\bar{f}(\bar{x}) \\ =& \frac{A\,V - a_1\,i - a_2\,i\,(P_s - P) - a_3\,i^2 - a_4\,i^2\,(P_s - P)}{(A\,X + V_0)^2}\left[A\,\beta^2\,(a_4\,i^2 + a_2\,i) + A^2\,\beta\,V\right] \end{aligned} \tag{4.13}$$

$$L_{\bar{g}}L_{\bar{f}}h(\bar{x}) = \frac{d(L_{\bar{f}}h(\bar{x}))}{d\bar{x}}\bar{g}(\bar{x}) = \frac{A\,\beta\,(a_1 + a_2\,(P_s - P) + 2\,a_3\,i + 2\,a_4\,i\,(P_s - P))}{A\,X + V_0} \tag{4.14}$$

$i < 0$:

$$L_{\bar{f}}^2 h(\bar{x}) = \frac{A\,V + b_1\,\bar{i} + b_2\,\bar{i}\,P + b_3\,\bar{i}^2 + b_4\,\bar{i}^2\,P}{(A\,X + V_0)^2}\left[A\,\beta^2\,(b_4\,\bar{i}^2 + b_2\,\bar{i}) + A^2\,\beta\,V\right] \tag{4.15}$$

$$L_{\bar{g}}L_{\bar{f}}h(\bar{x}) = -\frac{A\,\beta\,(b_1 + b_2\,P + 2\,b_3\,\bar{i} + 2\,b_4\,\bar{i}\,P)}{A\,X + V_0} \tag{4.16}$$

Because $L_{\bar{g}}L_{\bar{f}}h(\bar{x})$ is non-zero, no higher derivatives need to be taken and the relative degree of the extended system is $r = 2$. The derivatives can be formed into a linearized

system, which is a cascade of 2 integrators, with the final derivative set equal to ν as shown in Eq. (4.17) and Eq. (4.18).

$$\nu = \ddot{F} = L_{\bar{f}}^2 h(\bar{x}) + L_{\bar{g}} L_{\bar{f}} h(\bar{x}) w =$$

$i \geq 0$:

$$\begin{aligned} &= \frac{A\,V - a_1\,i - a_2\,i\,(P_s - P) - a_3\,i^2 - a_4\,i^2\,(P_s - P)}{(A\,X + V_0)^2}\,[A\,\beta^2\,(a_4\,i^2 + a_2\,i) + A^2\,\beta\,V] + \cdots \\ &\quad + \frac{A\,\beta\,(a_1 + a_2\,(P_s + P) + 2\,a_3\,i + 2\,a_4\,i\,(P_s - P))}{A\,X + V_0}\,w \end{aligned} \tag{4.17}$$

$i < 0$:

$$\begin{aligned} &= \frac{A\,V + b_1\,\bar{i} + b_2\,\bar{i}\,P + b_3\,\bar{i}^2 + b_4\,\bar{i}^2\,P}{(A\,X + V_0)^2}\,[A\,\beta^2\,(b_4\,\bar{i}^2 + b_2\,\bar{i}) + A^2\,\beta\,V] - \cdots \\ &\quad - \frac{A\,\beta\,(b_1 + b_2\,P + 2\,b_3\,\bar{i} - 2\,b_4\,\bar{i}\,P)}{A\,X + V_0}\,w \end{aligned} \tag{4.18}$$

Solving for w in Eq. (4.17) and Eq. (4.18), yields the control input of the affine system. The short-hand way of calculating w is from Eq. (2.13), which is applied to the system as shown in Eq. (4.19) and Eq. (4.20).

$$w = \frac{\nu - L_{\bar{f}}{}^{r} h(\bar{x})}{L_{\bar{g}} L_{\bar{f}}{}^{r-1} h(\bar{x})}$$

$i \geq 0$:

$$= \frac{\nu - \dfrac{A\,V - a_1\,i - a_2\,i\,(P_s - P) - a_3\,i^2 - a_4\,i^2\,(P_s - P)}{(A\,X + V_0)^2}\,[A\,\beta^2\,(a_4\,i^2 + a_2\,i) + A^2\,\beta\,V]}{\dfrac{A\,\beta\,(a_1 + a_2\,(P_s - P) + 2\,a_3\,i + 2\,a_4\,i\,(P_s - P))}{A\,X + V_0}} \tag{4.19}$$

$i < 0$:

$$= \frac{-\nu + \dfrac{A\,V + b_1\,\bar{i} + b_2\,\bar{i}\,P + b_3\,\bar{i}^2 + b_4\,\bar{i}^2\,P}{(A\,X + V_0)^2}\,[A\,\beta^2\,(b_4\,\bar{i}^2 + b_2\,\bar{i}) + A^2\,\beta\,V}{\dfrac{A\,\beta\,(b_1 + b_2\,P + 2\,b_3\,\bar{i} - 2\,b_4\,\bar{i}\,P)}{A\,X + V_0}} \tag{4.20}$$

K_1 and K_2 are designed to minimize the error between the desired force and the actual force according to Eq. (4.21). The gains selected based on experimental trials were: $K_1 = 10^5$ and $K_2 = 10^3$.

$$\nu = K_1\,(F_{desired} - F_{actual}) + K_2\,\frac{d(F_{desired} - F_{actual})}{dt} \tag{4.21}$$

The equation states are X, V, P, and i. These can be found by solving the original system in Eq. (4.8). In real time, X, the cylinder position, and P, the cylinder pressure, can be measured directly from the plant, because an in-cylinder position sensor and hydraulic pressure sensor would likely already be equipped on a combine harvester. The cylinder speed, V can be found by taking the time derivative of X with respect to time. Because the non-affine system was extended by defining a new input, the input current

is not calculated directly. To calculate the actual input current to the hydraulic valve, i, we just need to integrate Eq. (4.19) and Eq. (4.20) with respect to time.

To create the feedback linearization controller in Simulink, Eq. (4.19) and Eq. (4.20) can be put into *MATLAB Function* blocks along with the known parameters in Table 4.2. This can be done manually or via the *matlabFunctionBlock* command if the equations are already derived in MATLAB. A *switch* block can be used to control the discontinuity with the criterion set as $i \geq 0$. To get the input current, i the signal is fed through an integrator block with limits for the maximum current value. The Simulink diagram is shown in Fig. 4.11.

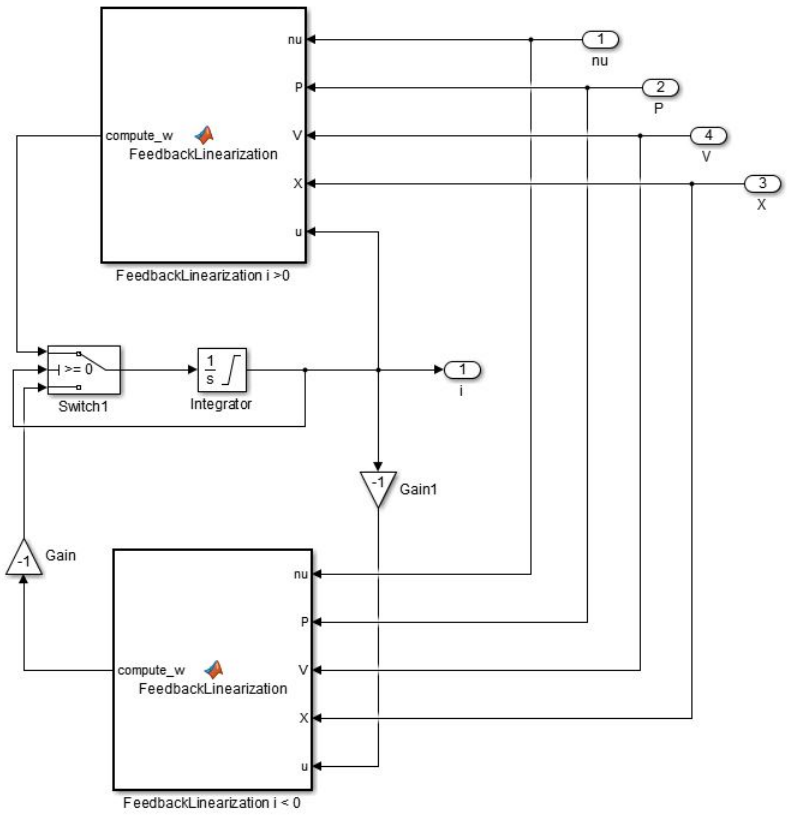

Figure 4.11: Simulink diagram of the feedback linearization controller.

4.3.2 Sensitivity dynamics

In order to adjust the input current to uncertainties and make the controller more robust, we need to first calculate the sensitivity with respect to the uncertain parameter or parameters. In this study, the uncertain parameter chosen is the hydraulic fluid bulk modulus. The bulk modulus describes the stiffness of a given volume of fluid. It is important in hydraulics because it affects the dynamics of the entire system and can vary widely. Many factors can affect the bulk modulus such as temperature, system pressure, and entrained air. To calculate the sensitivity dynamics with respect to the bulk modulus, the system in Eq. (4.8) is differentiated with respect to β, shown in Eq. (4.22). For simplicity, the subscript b will represent a full derivative with respect to β according to Eq. (2.18).

$$\begin{bmatrix} \dot{X}_b \\ \dot{V}_b \\ \dot{P}_b \\ \dot{i}_b \end{bmatrix} = \begin{bmatrix} V_b \\ \frac{1}{m}\left(P_b\,A - F_{load}\right) \\ Eq.\ (4.23)\ or\ Eq.\ (4.24) \\ 0 \end{bmatrix} + \begin{bmatrix} 0 \\ 0 \\ 0 \\ 1 \end{bmatrix} w_b$$

$$\begin{bmatrix} F_b \end{bmatrix} = \begin{bmatrix} P_b\,A \end{bmatrix} \tag{4.22}$$

$i \geq 0$:

$$\begin{aligned} \dot{P}_b =& \frac{a_1\,i + a_2\,i\,(P_s - P) + a_3\,i^2 + a_4\,i^2\,(P_s - P) - A\,V}{A\,X + V_0} - \cdots \\ & - \frac{A\,\beta\,(a_1\,i + a_2\,i\,(P_s - P) + a_3\,i^2 + a_4\,i^2\,(P_s - P) - A\,V)}{(A\,X + V_0)^2} X_b - \cdots \\ & - \frac{A\,\beta}{A\,X + V_0} V_b - \frac{\beta\,(a_2\,i + a_4\,i^2)}{A\,X + V_0} P_b + \frac{\beta\,(a_1 + a_2\,(P_s - P) + 2\,a_3\,i + a_4\,i\,(P_s - P)}{A\,X + V_0} i_b \end{aligned} \tag{4.23}$$

$$
\begin{aligned}
&i < 0: \\
&\dot{P}_b = -\frac{b_1\,\bar{i} + b_2\,\bar{i}\,P + b_3\,\bar{i}^2 + b_4\,\bar{i}^2\,P + A\,V}{A\,X + V_0} + \cdots \\
&\qquad + \frac{A\,\beta\,(b_1\,\bar{i} + b_2\,\bar{i}\,P + b_3\,\bar{i}^2 + b_4\,\bar{i}^2\,P + A\,V)}{(A\,X + V_0)^2} X_b - \cdots \\
&\qquad - \frac{A\,\beta}{A\,X + V_0} V_b - \frac{\beta\,(b_2\,\bar{i} + b_4\,\bar{i}^2)}{A\,X + V_0} P_b - \frac{\beta\,(b_1 + b_2\,P + 2\,b_3\,\bar{i} + 2\,b_4\,P\,\bar{i})}{A\,X + V_0} \bar{i}_b
\end{aligned}
\tag{4.24}
$$

The additional states from the sensitivity dynamics are X_b, V_b, P_b, and i_b. These can be found by augmenting the original system in Eq. (4.8) with the sensitivity dynamics in Eq. (4.22) and solving the entire system. In real time, P_b the pressure sensitivity, can be calculated by integrating Eq. (4.23) and Eq. (4.24) with respect to time. Because F_{load}, the force acting on the hydraulic cylinder, is not dependent on β, the same mechanical plant shown in Fig. 4.2 can be used to calculate X_b and V_b with input F_b. The easiest way to implement this is to linearize the mechanical plant about the operating point, which should be at the expected header height. The linearized system provides an accurate representation of the true system, because the force sensitivity is much less than the actual hydraulic forces going into the system and as a result, the system remains close to the operating point. Finally, calculating i_b, the input adjustment for sensitivity, will be explained in the next section.

The Simulink diagram of the sensitivity dynamics calculation is shown in Fig. 4.12. The diagram is set up in a similar way to the feedback linearization controller. *MATLAB function* blocks are used for Eq. (4.23) and Eq. (4.24) with a switch controlling the discontinuity. It's important to note that the criterion of the switch is still dependent on i and not i_b. The integration gives P_b, which when multiplied by A calculates F_b. This sensitivity force is fed into the linearized mechanical plant, which calculates X_b and V_b.

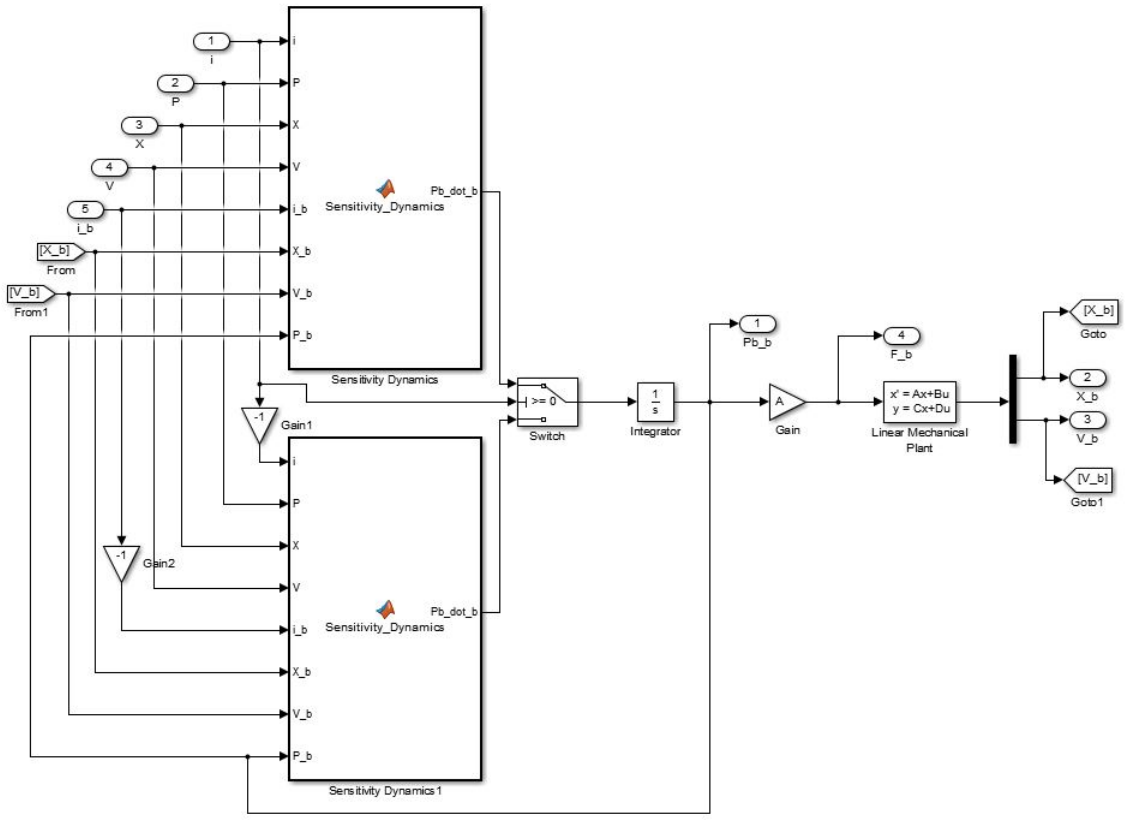

Figure 4.12: Simulink diagram of the sensitivity dynamics calculation.

4.3.3 Robust Feedback Linearization

To minimize the sensitivity, feedback linearization is used for the sensitivity augmented system. The simplest way of obtaining ν_b is by directly differentiating Eq. (4.17) and Eq. (4.18) with respect to β, according to Eq. (2.22):

$i \geq 0$

$$
\begin{aligned}
\nu_b = & \frac{A^2\,V\,(A\,V - a_3\,i^2 - a_1\,i + a_2\,i\,(P - P_s) + a_4\,i^2\,(P - P_s))}{(V_0 + A\,X)^2} \\
& + \frac{A\,w\,(a_1 - a_2\,(P - P_s) + 2\,a_3\,i - 2\,a_4\,i\,(P - P_s))}{V_0 + A\,X} \\
& + \frac{2\,A\,\beta\,(a_4\,i^2 + a_2\,i)\,(A\,V - a_3\,i^2 - a_1\,i + a_2\,i\,(P - P_s) + a_4\,i^2\,(P - P_s))}{(V_0 + A\,X)^2} \\
& - X_b \left(\frac{2\,A^3\,\beta\,V\,(A\,V - a_3\,i^2 - a_1\,i + a_2\,i\,(P - P_s) + a_4\,i^2\,(P - P_s))}{(V_0 + A\,X)^3} \right. \\
& + \frac{A^2\,\beta\,w\,(a_1 - a_2\,(P - P_s) + 2\,a_3\,i - 2\,a_4\,i\,(P - P_s))}{(V_0 + A\,X)^2} \\
& \left. + \frac{2\,A^2\,\beta^2\,(a_4\,i^2 + a_2\,i)\,(A\,V - a_3\,i^2 - a_1\,i + a_2\,i\,(P - P_s) + a_4\,i^2\,(P - P_s))}{(V_0 + A\,X)^3} \right) \\
& + V_b \left(\frac{A^3\,\beta\,V}{(V_0 + A\,X)^2} + \frac{A^2\,\beta^2\,(a_4\,i^2 + a_2\,i)}{(V_0 + A\,X)^2} \right. \\
& \left. + \frac{A^2\,\beta\,(A\,V - a_3\,i^2 - a_1\,i + a_2\,i\,(P - P_s) + a_4\,i^2\,(P - P_s))}{(V_0 + A\,X)^2} \right) \\
& + P_b \left(\frac{A\,\beta^2\,(a_4\,i^2 + a_2\,i)^2}{(V_0 + A\,X)^2} - \frac{A\,\beta\,w\,(a_2 + 2\,a_4\,i)}{V_0 + A\,X} + \frac{A^2\,\beta\,V\,(a_4\,i^2 + a_2\,i)}{(V_0 + A\,X)^2} \right) \\
& - i_b \left(\frac{A\,\beta^2\,(a_4\,i^2 + a_2\,i)\,(a_1 - a_2\,(P - P_s) + 2\,a_3\,i - 2\,a_4\,i\,(P - P_s))}{(V_0 + A\,X)^2} \right. \\
& + \frac{A^2\,\beta\,V\,(a_1 - a_2\,(P - P_s) + 2\,a_3\,i - 2\,a_4\,i\,(P - P_s)}{(V_0 + A\,X)^2} - \frac{A\,\beta\,w\,(2\,a_3 - 2\,a_4\,(P - P_s))}{(V_0 + A\,X)} \\
& \left. - \frac{A\,\beta^2\,(a_2 + 2\,a_4\,i)\,(A\,V - a_3\,i^2 - a_1\,i + a_2\,i\,(P - P_s) + a_4\,i^2\,(P - P_s))}{(V_0 + A\,X)^2} \right) \\
& + w_b \left(\frac{A\,\beta\,(a_1 - a_2\,(P - P_s) + 2\,a_3\,i - 2\,a_4\,i\,(P - P_s))}{V_0 + A\,X} \right)
\end{aligned}
\tag{4.25}
$$

$i < 0$

$$
\begin{aligned}
\nu_b = & \frac{A^2\,V\,(b_1\,i + b_3\,i^2 + A\,V + P\,b_2\,i + P\,b_4\,i^2)}{(V_0 + A\,X)^2} - \frac{A\,w\,(b_1 + P\,b_2 + 2\,b_3\,i + 2\,P\,b_4\,i)}{V_0 + A\,X} \\
& + \frac{2\,A\,\beta\,(b_4\,i^2 + b_2\,i)\,(b_1\,i + b_3\,i^2 + A\,V + P\,b_2\,i + P\,b_4\,i^2)}{(V_0 + A\,X)^2} \\
& - X_b \left(\frac{2\,A^3\,\beta\,V\,(b_1\,i + b_3\,i^2 + A\,V + P\,b_2\,i + P\,b_4\,i^2)}{(V_0 + A\,X)^3} \right. \\
& - \frac{A^2\,\beta\,w\,(b_1 + P\,b_2 + 2\,b_3\,i + 2\,P\,b_4\,i)}{(V_0 + A\,X)^2} \\
& \left. + \frac{2\,A^2\,\beta^2\,(b_4\,i^2 + b_2\,i)\,(b_1\,i + b_3\,i^2 + A\,V + P\,b_2\,i + P\,b_4\,i^2)}{(V_0 + A\,X)^3} \right) \\
& + V_b \left(\frac{A^3\,\beta\,V}{(V_0 + A\,X)^2} + \frac{A^2\,\beta^2\,(b_4\,i^2 + b_2\,i)}{(V_0 + A\,X)^2} \right. \\
& \left. + \frac{A^2\,\beta\,(b_1\,i + b_3\,i^2 + A\,V + P\,b_2\,i + P\,b_4\,i^2)}{(V_0 + A\,X)^2} \right) \\
& + P_b \left(\frac{A\,\beta^2\,(b_4\,i^2 + b_2\,i)^2}{(V_0 + A\,X)^2} - \frac{A\,\beta\,w\,(b_2 + 2\,b_4\,i)}{V_0 + A\,X} + \frac{A^2\,\beta\,V\,(b_4\,i^2 + b_2\,i)}{(V_0 + A\,X)^2} \right) \\
& + i_b \left(\frac{A\,\beta^2\,(b_4\,i^2 + b_2\,i)\,(b_1 + P\,b_2 + 2\,b_3\,i + 2\,P\,b_4\,i)}{(V_0 + A\,X)^2} \right. \\
& + \frac{A^2\,\beta\,V\,(b_1 + P\,b_2 + 2\,b_3\,i + 2\,P\,b_4\,i)}{(V_0 + A\,X)^2} - \frac{A\,\beta\,w\,(2\,b_3 + 2\,P\,b_4)}{V_0 + A\,X} \\
& \left. + \frac{A\,\beta^2\,(b_2 + 2\,b_4\,i)\,(b_1\,i + b_3\,i^2 + A\,V + P\,b_2\,i + P\,b_4\,i^2)}{(V_0 + A\,X)^2} \right) \\
& - w_b \left(\frac{A\,\beta\,(b_1 + P\,b_2 + 2\,b_3\,i + 2\,P\,b_4\,i)}{V_0 + A\,X} \right)
\end{aligned}
\tag{4.26}
$$

Solving for w_b in Eq. (4.25) and Eq. (4.26) yields the robust control adjustment for the affine system:

$$
\begin{aligned}
& i \geq 0 \\
w_b = & \frac{V_0 + A\,X}{A\,\beta\,(a_1 - a_2\,(P - P_s) + 2\,a_3\,i - 2\,a_4\,i\,(P - P_s))} \Bigg[\nu \\
& - \frac{A^2\,V\,(A\,V - a_3\,i^2 - a_1\,i + a_2\,i\,(P - P_s) + a_4\,i^2\,(P - P_s))}{(V_0 + A\,X)^2} \\
& - \frac{A\,w\,(a_1 - a_2\,(P - P_s) + 2\,a_3\,i - 2\,a_4\,i\,(P - P_s))}{V_0 + A\,X} \\
& - \frac{2\,A\,\beta\,(a_4\,i^2 + a_2\,i)\,(A\,V - a_3\,i^2 - a_1\,i + a_2\,i\,(P - P_s) + a_4\,i^2\,(P - P_s))}{(V_0 + A\,X)^2} \\
& + X_b \left(\frac{2\,A^3\,\beta\,V\,(A\,V - a_3\,i^2 - a_1\,i + a_2\,i\,(P - P_s) + a_4\,i^2\,(P - P_s))}{(V_0 + A\,X)^3} \right. \\
& + \frac{A^2\,\beta\,w\,(a_1 - a_2\,(P - P_s) + 2\,a_3\,i - 2\,a_4\,i\,(P - P_s))}{(V_0 + A\,X)^2} \\
& \left. + \frac{2\,A^2\,\beta^2\,(a_4\,i^2 + a_2\,i)\,(A\,V - a_3\,i^2 - a_1\,i + a_2\,i\,(P - P_s) + a_4\,i^2\,(P - P_s))}{(V_0 + A\,X)^3} \right) \\
& - V_b \left(\frac{A^3\,\beta\,V}{(V_0 + A\,X)^2} + \frac{A^2\,\beta^2\,(a_4\,i^2 + a_2\,i)}{(V_0 + A\,X)^2} \right. \\
& \left. + \frac{A^2\,\beta\,(A\,V - a_3\,i^2 - a_1\,i + a_2\,i\,(P - P_s) + a_4\,i^2\,(P - P_s))}{(V_0 + A\,X)^2} \right) \\
& - P_b \left(\frac{A\,\beta^2\,(a_4\,i^2 + a_2\,i)^2}{(V_0 + A\,X)^2} - \frac{A\,\beta\,w\,(a_2 + 2\,a_4\,i)}{V_0 + A\,X} + \frac{A^2\,\beta\,V\,(a_4\,i^2 + a_2\,i)}{(V_0 + A\,X)^2} \right) \\
& + i_b \left(\frac{A\,\beta^2\,(a_4\,i^2 + a_2\,i)\,(a_1 - a_2\,(P - P_s) + 2\,a_3\,i - 2\,a_4\,i\,(P - P_s))}{(V_0 + A\,X)^2} \right. \\
& + \frac{A^2\,\beta\,V\,(a_1 - a_2\,(P - P_s) + 2\,a_3\,i - 2\,a_4\,i\,(P - P_s)}{(V_0 + A\,X)^2} - \frac{A\,\beta\,w\,(2\,a_3 - 2\,a_4\,(P - P_s))}{(V_0 + A\,X)} \\
& \left. - \frac{A\,\beta^2\,(a_2 + 2\,a_4\,i)\,(A\,V - a_3\,i^2 - a_1\,i + a_2\,i\,(P - P_s) + a_4\,i^2\,(P - P_s))}{(V_0 + A\,X)^2} \right) \Bigg]
\end{aligned}
\tag{4.27}
$$

$i < 0$

$$
\begin{aligned}
w_b = {} & \frac{V_0 + A\,X}{A\,\beta\,(b_1 + P\,b_2 + 2\,b_3\,i + 2\,P\,b_4\,i)} V_0 + A\,X \Bigg[- \nu \\
& + \frac{A^2\,V\,(b_1\,i + b_3\,i^2 + A\,V + P\,b_2\,i + P\,b_4\,i^2)}{(V_0 + A\,X)^2} - \frac{A\,w\,(b_1 + P\,b_2 + 2\,b_3\,i + 2\,P\,b_4\,i)}{V_0 + A\,X} \\
& + \frac{2\,A\,\beta\,(b_4\,i^2 + b_2\,i)\,(b_1\,i + b_3\,i^2 + A\,V + P\,b_2\,i + P\,b_4\,i^2)}{(V_0 + A\,X)^2} \\
& - X_b \Bigg(\frac{2\,A^3\,\beta\,V\,(b_1\,i + b_3\,i^2 + A\,V + P\,b_2\,i + P\,b_4\,i^2)}{(V_0 + A\,X)^3} \\
& - \frac{A^2\,\beta\,w\,(b_1 + P\,b_2 + 2\,b_3\,i + 2\,P\,b_4\,i)}{(V_0 + A\,X)^2} \\
& + \frac{2\,A^2\,\beta^2\,(b_4\,i^2 + b_2\,i)\,(b_1\,i + b_3\,i^2 + A\,V + P\,b_2\,i + P\,b_4\,i^2)}{(V_0 + A\,X)^3} \Bigg) \\
& + V_b \Bigg(\frac{A^3\,\beta\,V}{(V_0 + A\,X)^2} + \frac{A^2\,\beta^2\,(b_4\,i^2 + b_2\,i)}{(V_0 + A\,X)^2} \\
& + \frac{A^2\,\beta\,(b_1\,i + b_3\,i^2 + A\,V + P\,b_2\,i + P\,b_4\,i^2)}{(V_0 + A\,X)^2} \Bigg) \\
& + P_b \Bigg(\frac{A\,\beta^2\,(b_4\,i^2 + b_2\,i)^2}{(V_0 + A\,X)^2} - \frac{A\,\beta\,w\,(b_2 + 2\,b_4\,i)}{V_0 + A\,X} + \frac{A^2\,\beta\,V\,(b_4\,i^2 + b_2\,i)}{(V_0 + A\,X)^2} \Bigg) \\
& + i_b \Bigg(\frac{A\,\beta^2\,(b_4\,i^2 + b_2\,i)\,(b_1 + P\,b_2 + 2\,b_3\,i + 2\,P\,b_4\,i)}{(V_0 + A\,X)^2} \\
& + \frac{A^2\,\beta\,V\,(b_1 + P\,b_2 + 2\,b_3\,i + 2\,P\,b_4\,i)}{(V_0 + A\,X)^2} - \frac{A\,\beta\,w\,(2\,b_3 + 2\,P\,b_4)}{V_0 + A\,X} \\
& + \frac{A\,\beta^2\,(b_2 + 2\,b_4\,i)\,(b_1\,i + b_3\,i^2 + A\,V + P\,b_2\,i + P\,b_4\,i^2)}{(V_0 + A\,X)^2} \Bigg) \Bigg]
\end{aligned}
\tag{4.28}
$$

The input current adjustment i_b is found by integrating Eq. (4.27) and Eq. (4.28) with respect to time. K_{b_1} and K_{b_2} are designed to stabilize the sensitivity output according to

to Eq. (4.29). In general, the same gains of the nominal feedback linearization controller provide a good starting point for the sensitivity gains, though it was found through experimentation that the sensitivity gains could be increased higher before chattering occurs. The gains selected were: $K_{b_1} = 5 \times 10^6$ and $K_{b_2} = 5 \times 10^4$.

$$\nu_b = -K_{b_1} F_b - K_{b_2} \frac{dF_b}{dt} \tag{4.29}$$

To implement the input adjustment controller in Simulink, it is set up similar to the nominal feedback linearization controller. *MATLAB function* blocks are used for Eq. (4.27) and Eq. (4.28) with the additional sensitivity states, as well as i, w, and ν_b. A switch is used to evauluate the criterion with i and the output is integrated to calculate i_b, which is fed back into the input adjustment calculation. The simulink diagram is shown in Fig 4.13.

The complete robust feedback linearization controller includes the nominal controller computed in Eq. (4.19) and Eq. (4.20), the sensitivity dynamics in Eq. (4.22), and the input adjustment for sensitivity robustness in Eq. (4.27) and Eq. (4.28). Additionally, four gains were chosen in calculating ν and ν_b according to Eq. (4.21) and Eq. (4.29) to stabilize the system. The complete Simulink diagram for this is shown in Fig. 4.14. Here the final input to the hydraulic plant is given by the summation of the nominal feedback linearization controller and the input adjustment calculation. For simplicity, the gains in the ν and ν_b calculations are put into the system using a *PID Controller* block, with $K_P = K_1$, $K_I = 0$, and $K_D = K_2$. This could have also been implemented using *gain* blocks and differentiating the signal with a *derivative* block for K_2.

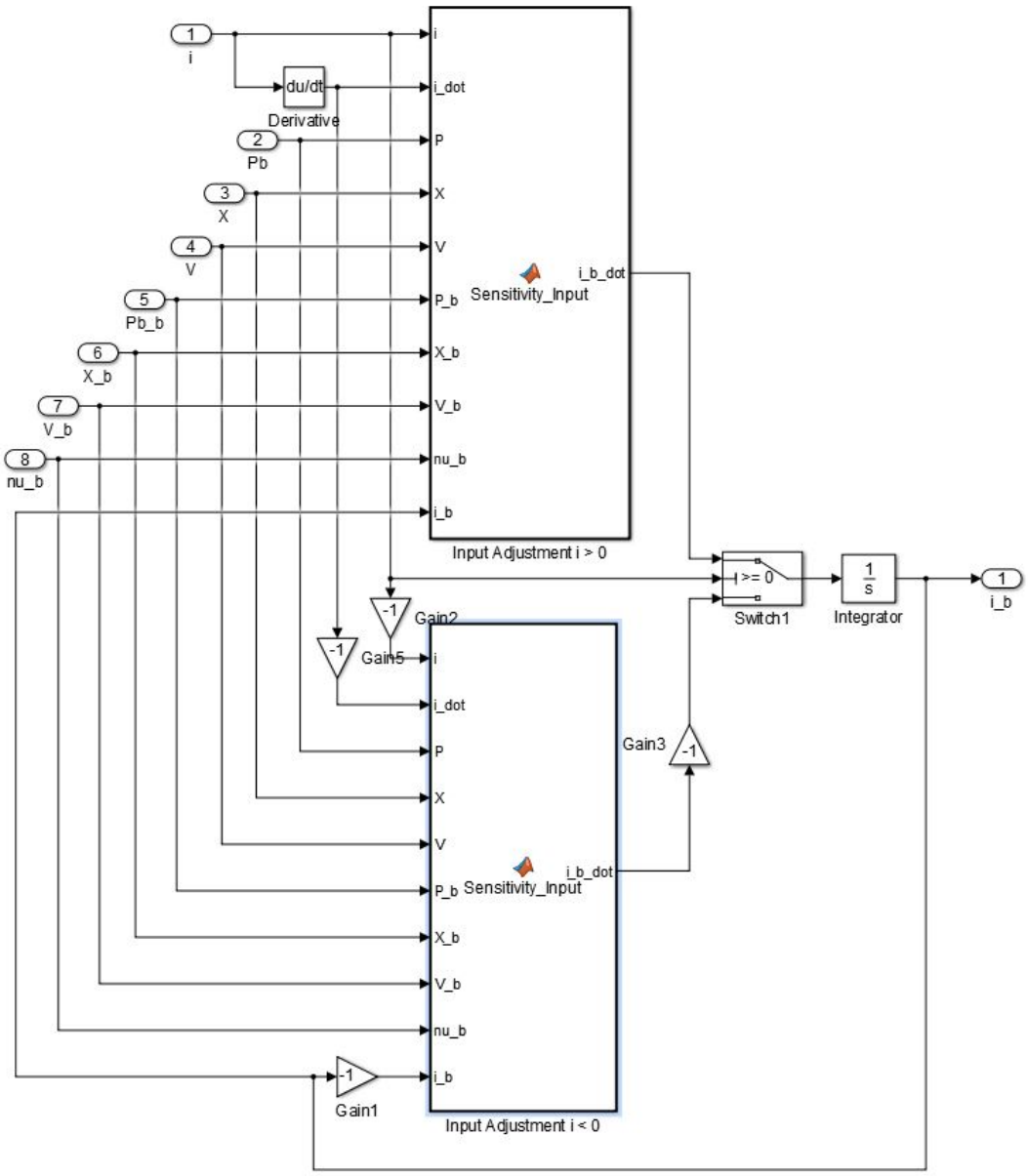

Figure 4.13: Simulink diagram of the robust input adjustment controller.

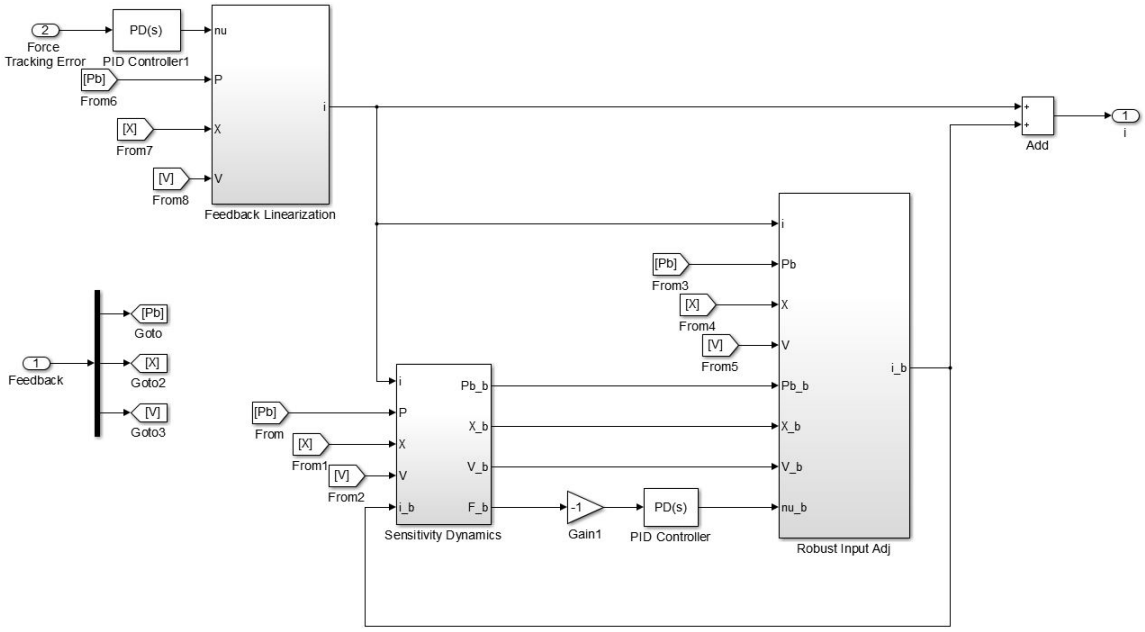

Figure 4.14: Simulink diagram of the complete robust feedback linearization controller.

4.4 Results

A closed loop system was simulated in Simulink for the combine header lift system. The system includes the Integrated Robust Optimal Design (IROD) controller designed in [1,22], the robust feedback linearization (RFL) controller designed in the previous section, and the hydraulic and mechanical plant models. The combine terrain is modeled as a sinusoidal surface with varying amplitudes and frequencies. Because the sinusoidal frequency is a function of both the vehicle travel speed and the terrain profile, we will instead specify the terrain period, with units of length, and vehicle travel speed separately. With any given pair, the input frequency can be calculated as shown in Table 4.4. Even though the frequency of any pair is not unique, the time delay between the header and the front and rear wheels is only dependent on the terrain period. For this reason, two conditions may have the same input frequency, but the combine will respond differently. For example, driving slowly over steep terrain will be different than driving quickly over gradual terrain, despite going over the peaks and valleys at the same rate.

Table 4.4: Conversion table for combine travel speed and terrain period to equivalent frequency in Hertz.

		Terrain Period			
		7m	**15m**	**25m**	**35m**
Vehicle Speed	**1**	0.401	0.187	0.112	0.080
	2	0.803	0.375	0.225	0.161
	3	1.204	0.562	0.337	0.241
	4	1.605	0.749	0.449	0.321
	5	2.006	0.936	0.562	0.401
	6	2.408	1.124	0.674	0.482
	7	2.809	1.311	0.786	0.562
	8	3.210	1.498	0.899	0.642
	9	4.013	1.873	1.124	0.803

Figure 4.15 shows the simulation plots for the IROD/RFL controller under the following condition: terrain period = 15m, terrain amplitude = 0.15m, travel speed = 6mph.

The plots show accurate header height tracking with an RMS error of 0.83cm or 5.5 percent of the terrain amplitude and a maximum error of 4.28cm. The RFL controller tracked the desired hydraulic force very well with an actual force RMS error of 55N or 0.044 percent of the desired force.

Figure 4.16 shows the difference between nominal feedback linearization and robust feedback linearization by comparing the force sensitivity with respect to the bulk modulus. The nominal system is tested by disconnecting the sensitivity adjustment i_b and plotting the force sensitivity from the sensitivity dynamics. It can be seen from the figure that for the given condition, the RMS sensitivity decreases from 1.919×10^{-6} to 6.009×10^{-9}, an improvement of 99.7 percent. To put that in perspective, if the bulk modulus decreases from 1.45×10^{9} to 3.625×10^{8}, a decrease of 75 percent caused by 1 percent of entrained air [33], the actual force output of the hydraulic cylinder would be off by 2,087N on average for the nominal feedback linearizion system. This could cause major tracking and stability issues. For the robust system this change in bulk modulus would only cause a 6.53N change in the hydraulic force on average. To compare the cost of decreased sensitivity, we can compare the performance of the nominal feedback linearization and see how it differs from the robust feedback linearization under the same conditions. The performance plots of the nominal system are shown in Fig. 4.17. The plots show that the effect in performance is very small. There is a slight decrease in the hydraulic force tracking of the robust system (52N - Nominal, 55N - Robust), but has no noticeable impact on the overall header height tracking.

To test a lower frequency and higher amplitude case, simulation was run for the nominal and robust controllers with the following conditions: terrain period = 35m, terrain amplitude = 1.0m, travel speed = 3mph. The IROD/RFL performance plot is shown in Fig 4.18, with similar height and force tracking as the previous condition. The sensitivity plots of the nominal and robust controllers are shown in Fig. 4.19, which show a similar sensitivity improvement of 98.1 percent. Figure 4.20 shows the performance

of the nominal controller, which is nearly equivalent to the robust controller, thus the robust input adjustment for sensitivity has no noticeable impact on the header height tracking performance.

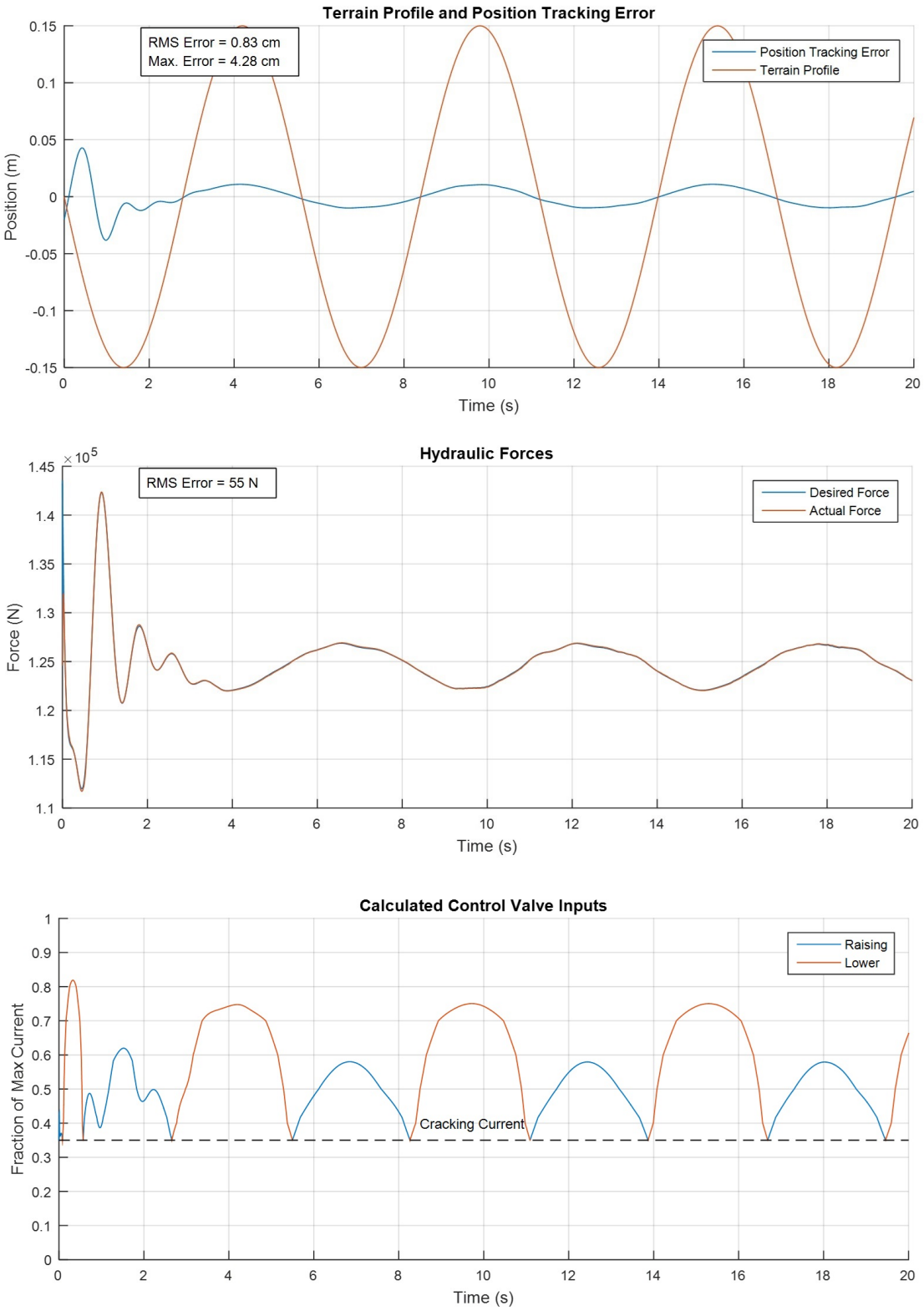

Figure 4.15: Simulation plots for IROD/RFL controller with terrain period = 15m, terrain amplitude = 0.15m, travel speed = 6mph.

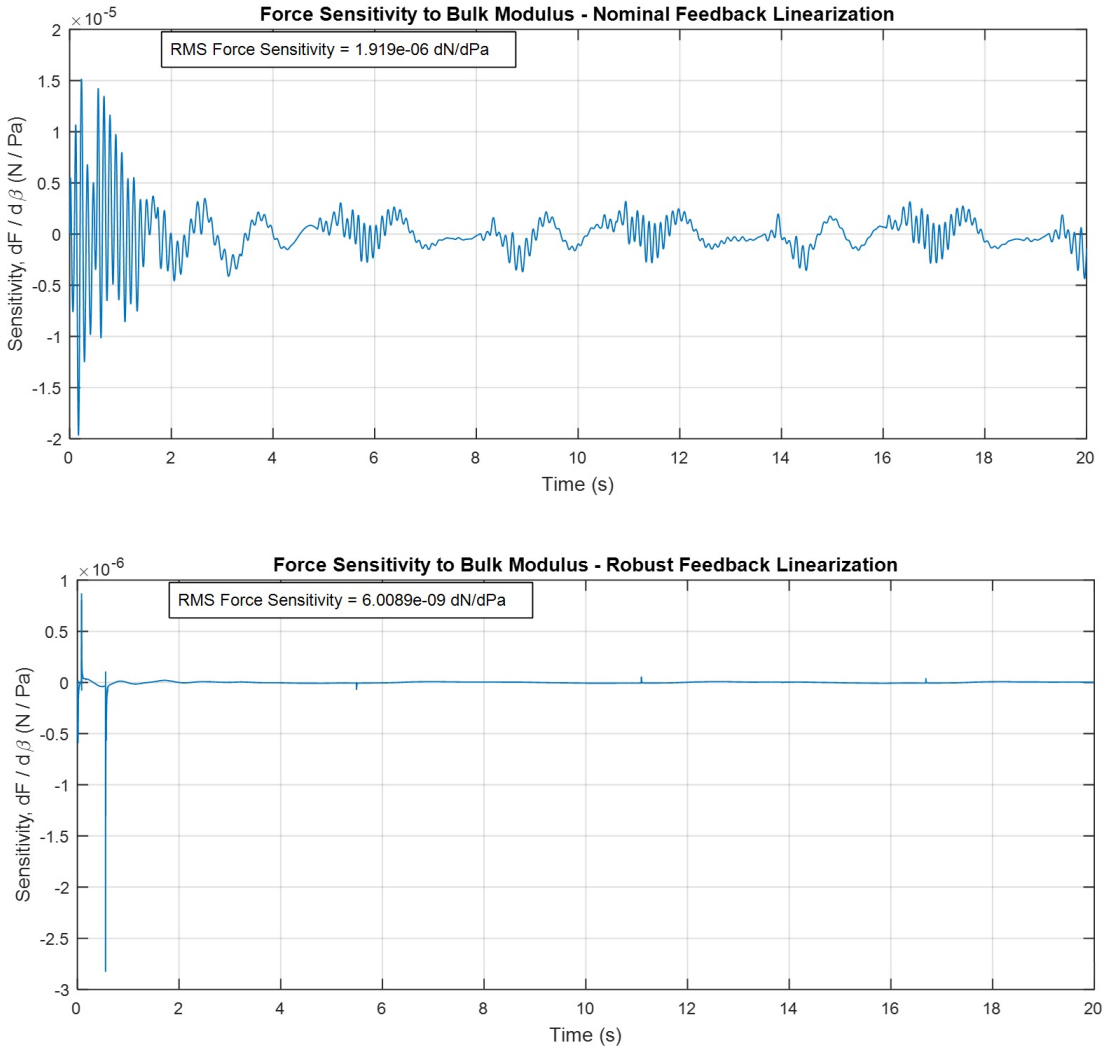

Figure 4.16: Comparing force sensitivity of nominal and robust feedback linearization with terrain period = 15m, terrain amplitude = 0.15m, travel speed = 6mph.

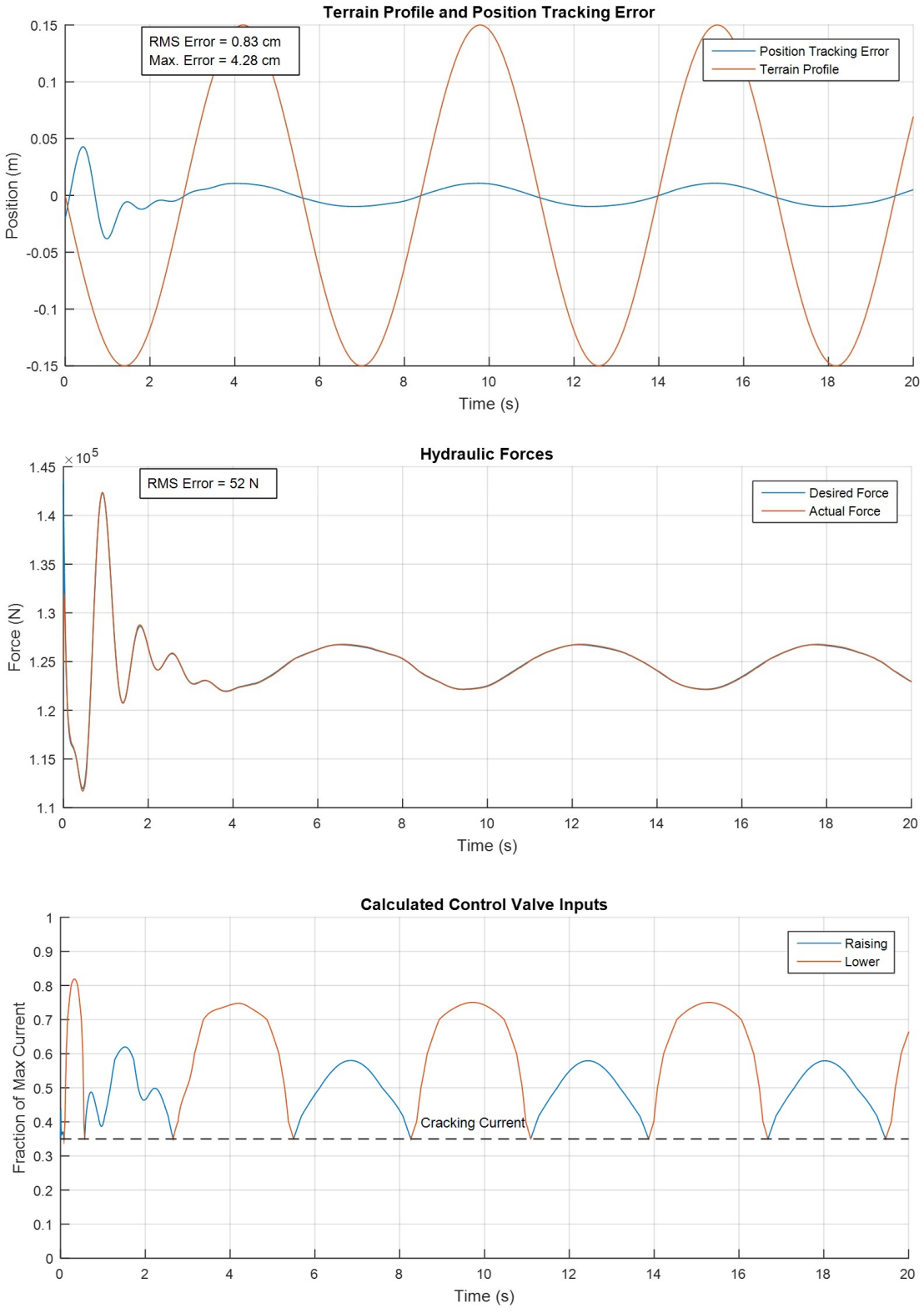

Figure 4.17: Simulation plots for IROD and nominal feedback linearization controller with terrain period = 15m, terrain amplitude = 0.15m, travel speed = 6mph.

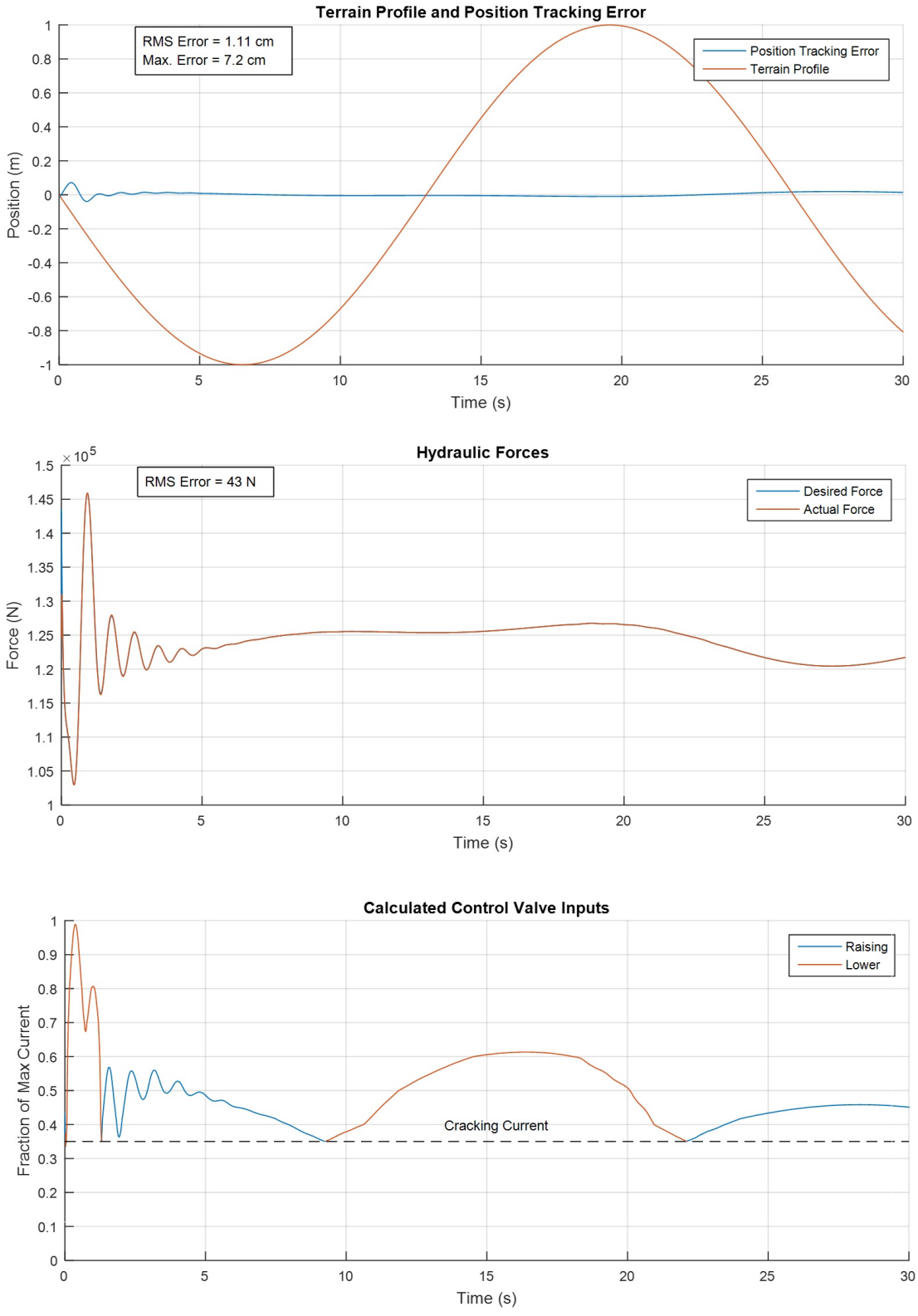

Figure 4.18: Simulation plots for IROD/RFL controller with terrain period = 35m, terrain amplitude = 1.0m, travel speed = 3mph.

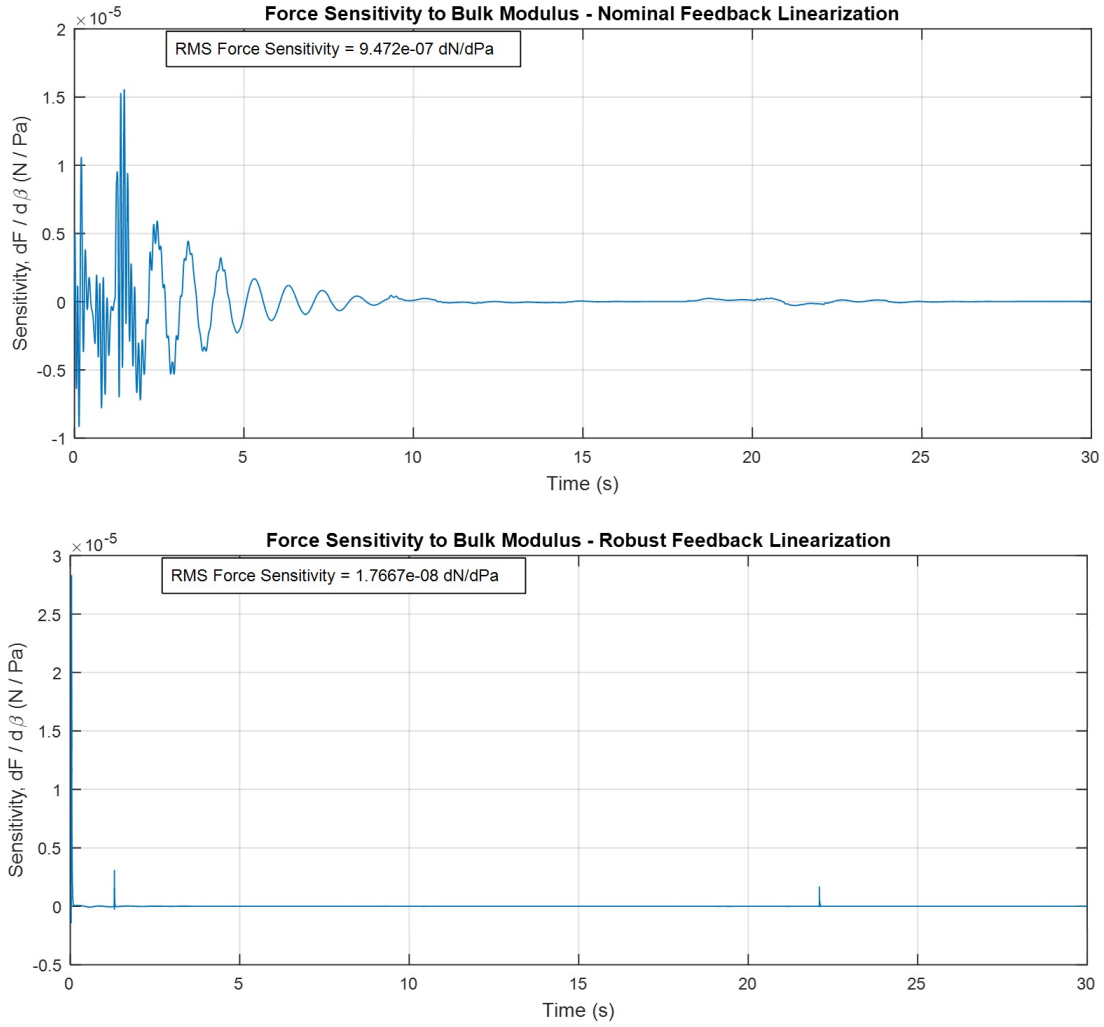

Figure 4.19: Comparing force sensitivity of nominal and robust feedback linearization with terrain period = 35m, terrain amplitude = 1.0m, travel speed = 3mph.

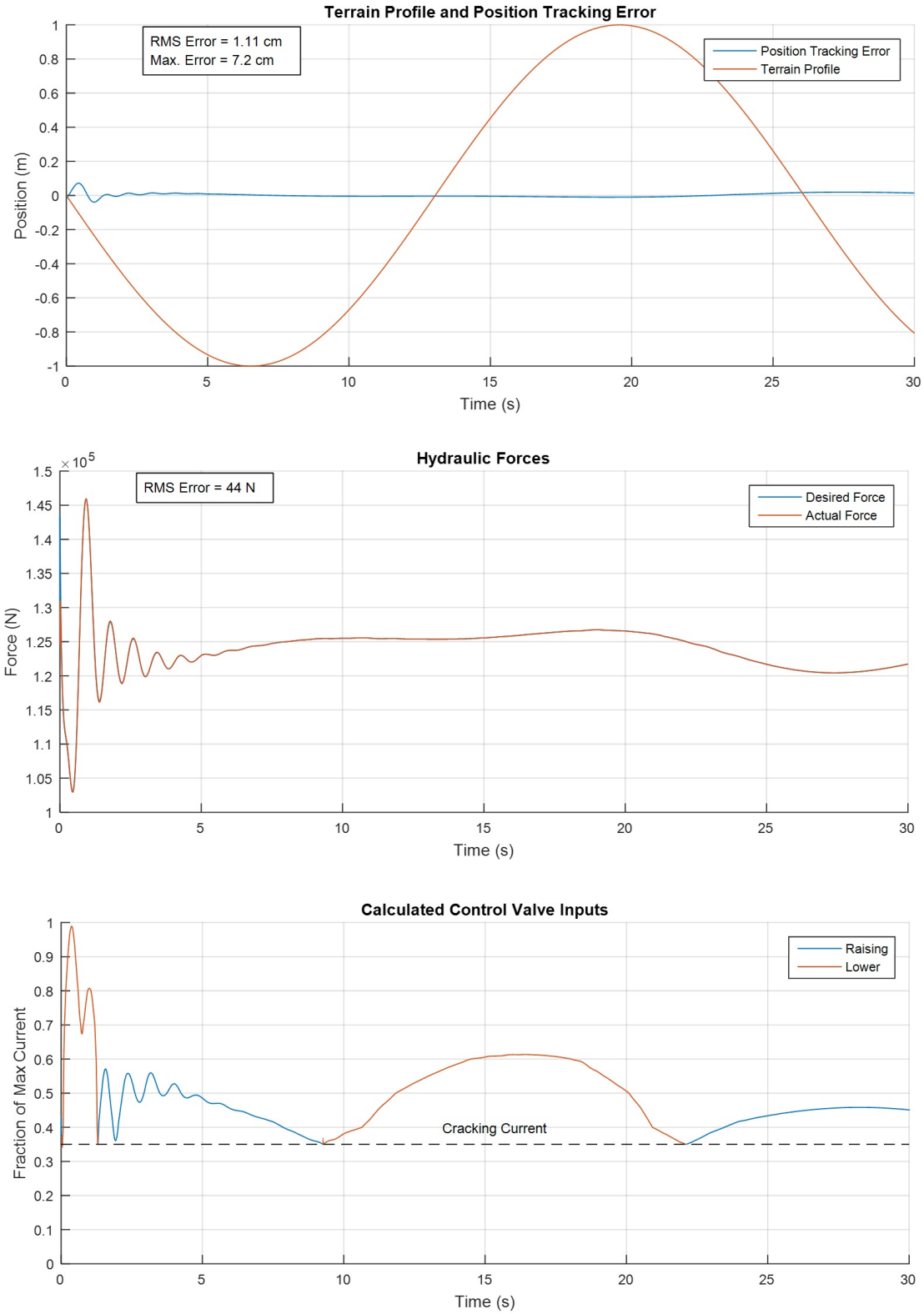

Figure 4.20: Simulation plots for IROD and nominal feedback linearization controller with terrain period = 35m, terrain amplitude = 1.0m, travel speed = 3mph.

To benchmark the performance of the control system designed in this study, it was compared to a PID controller, which is commonly used in industry. For the PID system, both the IROD and the robust feedback linearizing controller are replaced with a single PID controller as shown in Fig 4.21. The input to the controller is the header height tracking error and the output is the control current to the poppet valves. The gains were initially tuned using the MATLAB Control Design toolbox. The toolbox automatically linearized the plants and selected gains based on a standard step input for best reference tracking. Then the gains were manually tuned by simulation under the same conditions that would be used for the final simulation tests. The final gains selected were: $K_p = 1.2$, $K_I = 1.6$, and $K_D = -0.4$. Note that this controller is likely much more aggressive that would normally be used in this application, where it is common to use only a PI controller for robust purposes, but we wanted to provide the best possible reference tracking for a PID controller under the tested conditions for benchmarking.

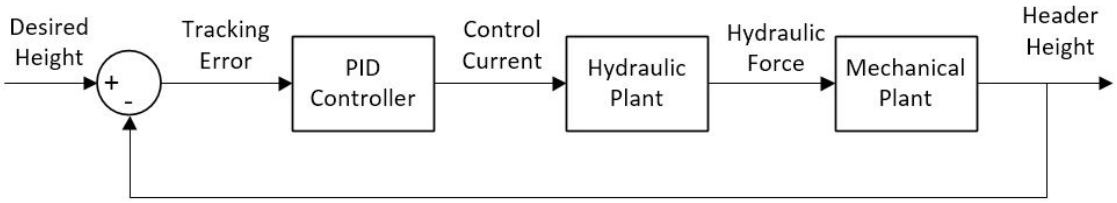

Figure 4.21: Control structure of PID system for performance comparison.

The PID and the IROD/RFL controllers were simulated under a variety of identical conditions. The simulations varied three parameters over 105 total simulations: combine travel speed (1-10 mph), terrain sinusoidal amplitude (0.1 - 1.0 m), and terrain period (7 - 35 m). The simulation time was set to 60 seconds and RMS height tracking error and the mean fluid power were tabulated for every test. The fluid power was calculated

from the product of cylinder pressure and flow rate. Because the lift cylinder is a single acting cylinder, the power is non-zero only when $i > 0$. When $i \leq 0$ the fluid is forced out of the cylinder due to gravity, and besides the negligible electrical power to the control valve, no power is used. Additionally, for the IROD/RFL system, RMS force tracking error and RMS force sensitivity were also tabulated to verify the performance of just the RFL controller compared to the nominal feedback linearization controller.

Figures 4.22, 4.23, 4.24, and 4.25 show the overall height tracking error of the PID and IROD/RFL systems for 7m, 15m, 25m, and 35m terrain periods respectively, at various terrain amplitudes and combine travel speeds. These plots show significantly better header height tracking with the IROD/RFL controller compared to the PID controller, where the IROD/RFL controller performed better in all 105 different simulations. In fact, it can be seen that under the same ground conditions, the IROD/RFL controller performed better at 10mph than the PID did at 2mph. Table 4.5 give the average performance summary over all tested conditions for the PID and IROD/RFL controllers. It shows that the IROD/RFL controller improves the header height tracking RMS error by 84.1 percent and the maximum error by 71.1 percent with 4.05 percent less power input compared to the PID controller.

Even though the results show that with the IROD/RFL controller combine harvesters can travel over five times as fast with the same tracking tolerance, combines currently do not have the capacity to travel at speeds up to 10mph while harvesting. To verify performance over conditions which a typical combine would be harvesting, Table 4.6 shows a summary of tests where the travel speed was 5mph or less. This table shows that the improvements of the slower speeds are nearly identical to the overall improvements in Table 4.5. This implies that the header height tracking improvement is not a function of the speed, but a user can expect approximately an 84 percent improvement in the RMS error over all speed ranges.

Table 4.7 compares the performance of the IROD/RFL and the IROD/nominal feed-

back linearization controller without the sensitivity adjustment. It shows that the robust controller improves the sensitivity with respect to the bulk modulus by an average of 98.8 percent over all 105 simulations. By also comparing height tracking error, force tracking error, and fluid power, it is seen that there is no decrease in performance when adding the robust adjustment to the controller. This shows that besides the additional development, there is no additional cost for the robust controller compared to nominal feedback linearization.

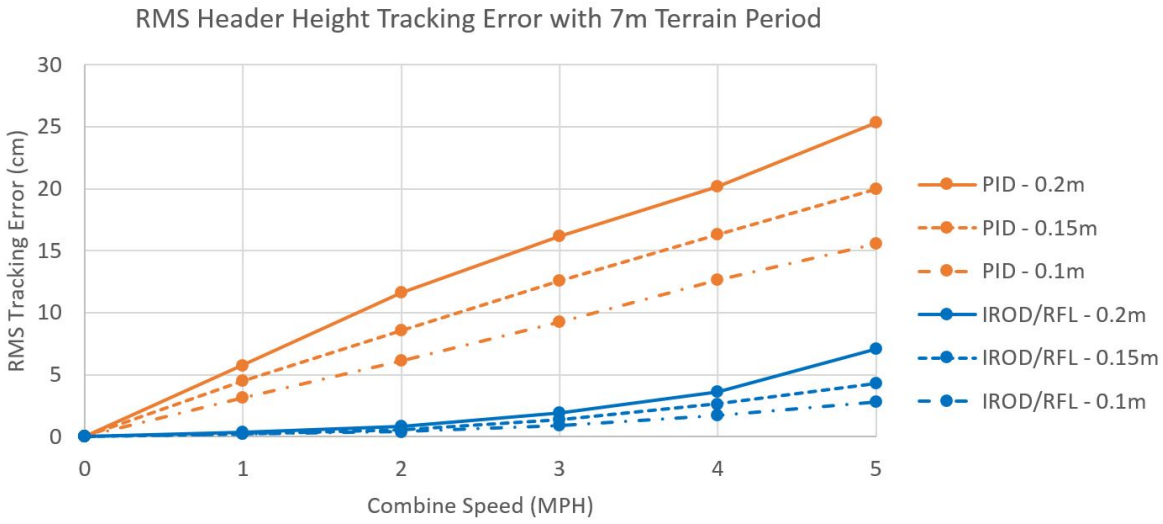

Figure 4.22: Comparison between header height tracking error of IROD/RFL and PID controllers at 7m terrain period and various travel speeds and terrain amplitudes.

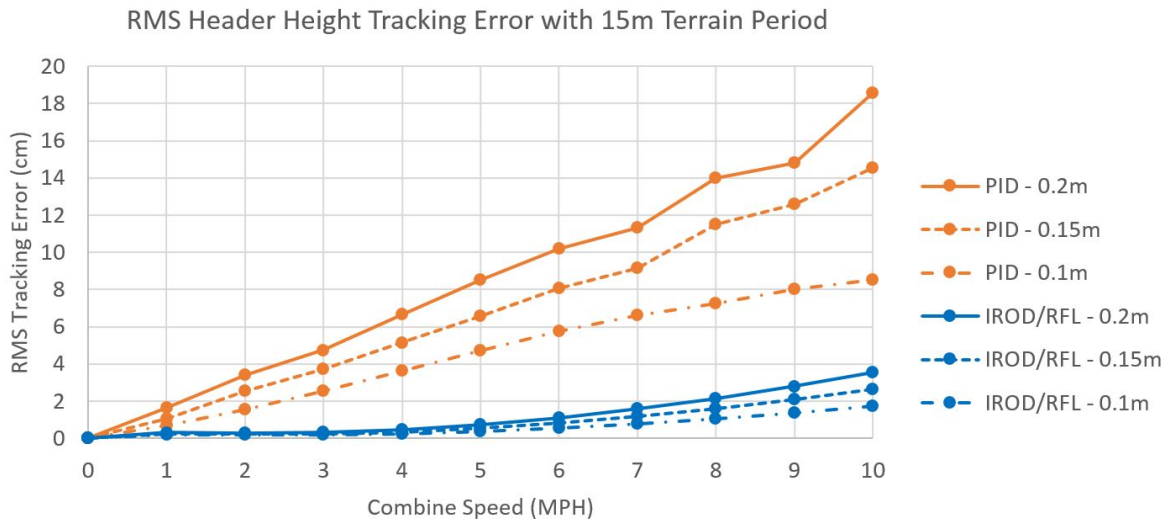

Figure 4.23: Comparison between header height tracking error of IROD/RFL and PID controllers at 15m terrain period and various travel speeds and terrain amplitudes.

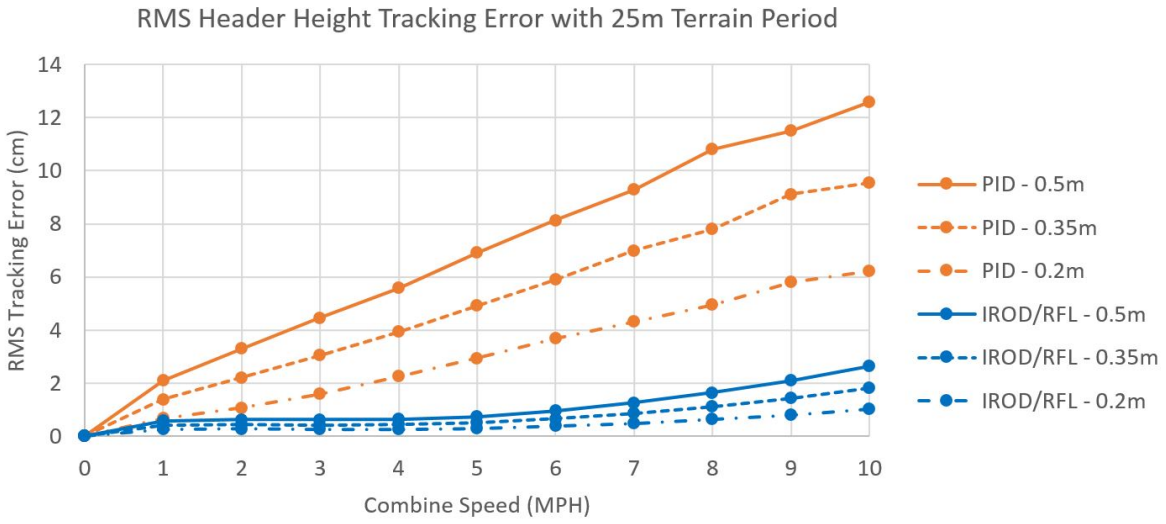

Figure 4.24: Comparison between header height tracking error of IROD/RFL and PID controllers at 25m terrain period and various travel speeds and terrain amplitudes.

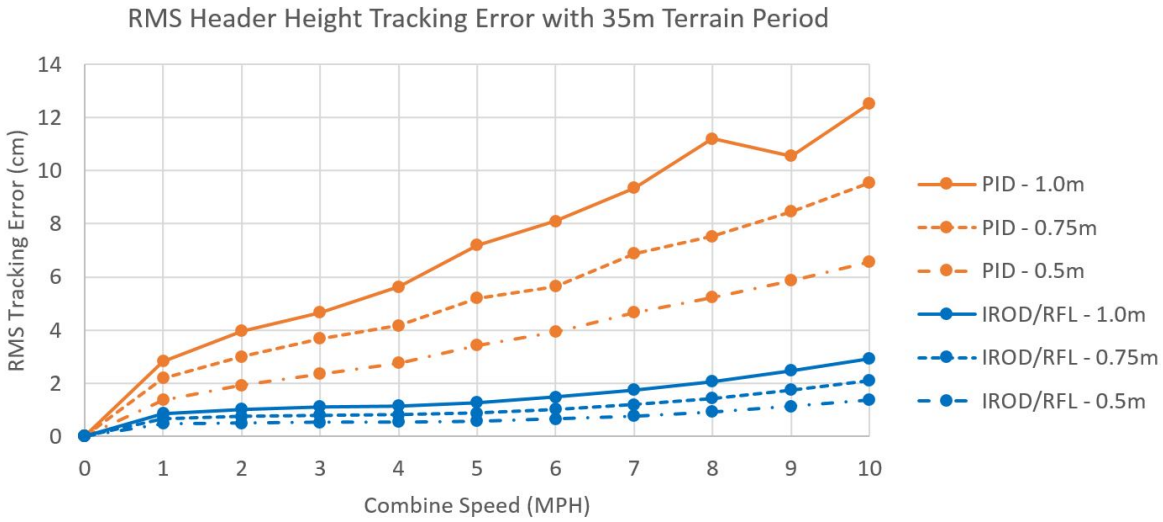

Figure 4.25: Comparison between header height tracking error of IROD/RFL and PID controllers at 35m terrain period and various travel speeds and terrain amplitudes.

Table 4.5: Performance comparison of IROD/RFL to PID over all tested conditions.

Metric	**PID**	**IROD/RFL**	**Improvement**
Height Tracking RMS Error	7.73 cm	1.23 cm	84.1%
Height Tracking Max Error	21.08 cm	6.10 cm	71.1%
Fluid Power	2.22 kW	2.13 kW	4.05%

Table 4.6: Performance comparison of IROD/RFL to PID where vehicle speed is 5mph or less.

Metric	**PID**	**IROD/RFL**	**Improvement**
Height Tracking RMS Error	5.76 cm	0.88 cm	84.7%
Height Tracking Max Error	17.33 cm	4.27 cm	75.4%
Fluid Power	1.69 kW	1.64 kW	2.96%

Table 4.7: Performance comparison of the nominal controller and robust controller over all test conditions.

Metric	**Nominal**	**Robust**	**Improvement**
Height Tracking RMS Error	1.2309 cm	1.2302 cm	0.06%
Height Tracking Max Error	6.1037 cm	6.1018 cm	0.03%
Force Tracking Error	259.01 N	258.03 N	0.38%
Fluid Power	2.134 kW	2.130 kW	0.19%
Force Sensitivity	$2.03 \times 10^{-6} \frac{N}{Pa}$	$2.40 \times 10^{-8} \frac{N}{Pa}$	98.8%

CHAPTER 5. SUMMARY AND FUTURE WORK

The primary focus of this research work has been extending the robust feedback linearization (RFL) methodology to control non-affine systems and applying it to the combine harvester header height problem. Feedback linearization is often the best controller for systems with minimum phase zero dynamics and are feedback linearizable, but it is traditionally known for not being robust to parameter variations. The methodology presented in this work uses sensitivity dynamics to adjust the input to minimize the effects of parametric uncertainties on the system. Previously, RFL could only be applied to control affine non-linear systems, but this research expands the nominal and robust controllers to the control non-affine systems as well, by extending the states and defining a new input to the system. This increases the relative degree of the system by one and does not solve for the initial input directly, but this can easily be accounted for by integrating the calculated input.

The RFL method is ideally suited for hydraulically actuated systems and can be used in conjuction with previous work on integrated robust optimal design (IROD) to design a controller for a complete hydraulically controlled multi-body system. A general design methodology is proposed in this work and is applied to the combine harvester header height problem. Rigorous simulation testing showed that the IROD/RFL controller can achieve very accurate header height tracking. It was compared to a PID controlled system, which is commonly used in industry, and the IROD/RFL proved to have much better tracking with lower input power. This could effectively reduce harvest yield losses and increase harvest speed and productivity, which could save the agricultural producer

on the bottom line as well as the consumer. Adding the robust adjustment to the control input significantly reduced the sensitivity to the chosen uncertain parameter, the bulk modulus. Comparing the performance of the nominal and robust system, it was seen that adding the robust aspect did not diminish tracking performance.

The contributions of this work addressed implementation concerns by simplifying the design process and increasing the usability. The major contributions of this thesis are:

1. Extending the methodology to control non-affine systems
    - Hydraulic valve dynamics are rarely input affine and exhibit non-linear behavior.
    - The example shown in Chapter 4 has an input with degree 2, and could be expanded for higher degrees as well.
2. Defining the input as control current instead of spool/poppet valve position
    - Although certain valves (servovalves) do have spool/poppet closed-loop feedback, this comes at an added expense and is not generally used in the mobile equipment industry.
    - Control current is the true input into the hydraulic plant and requires no separate controller or conversion.
3. Reducing complexity involving the hydraulic equations of motion
    - Early feedback suggested that design engineers in industry rarely if ever deal with hydraulic equations of motion for valve dynamics.
    - The valve equations were replaced with flow diagrams/tables directly from the manufacturer, which do not require knowledge of actual valve specifications.
    - The hydraulic actuator equation was still used, but this is more standardized over all sizes and types and contains measurable parameters.

The work presented here has made significant improvements in the development of IROD/RFL, but there are still opportunities for improvement before implementing the methodology for off-highway mobile equipment. Even though feedback linearization has been made more robust to parametric uncertainties, it is still sensitivity to time delays. This did not pose a problem for simulations, but in a physical system there will be small time delays in the electronics and software architecture, which could cause tracking or stability issues. There is a large amount of research on the topic of addressing time delays in closed-loop systems and could be added to this controller. Similarly, it would be good to include the valve dynamics, which could be included as a lowpass filter according to the manufacturers specifications. This was not included in this study because of the lack of time delay compensation. The simulations in this study were run in continuous time, but using a discrete time system would bring it one step closer to implementation. Mobile equipment often use CAN bus for networking and communication for sensors and controllers on the machine. CAN bus is a message based protocol which sends specific information over a preset transmission rate, essentially acting as a discrete time system with a fixed step size. The next step would be to implement a hardware in the loop test using physical controllers and communication methods, but closing the loop with the simulated plants. Finally, the IROD/RFL controller can be tested on a physical machine.

Expansion of the work could involve applying the IROD/RFL controller to different applications. Possible applications include: smart feedrate control for cotton harvesting, bucket level control for a wheel loader, and automatic boom height control for an agricultural sprayer, among many others. To encourage industry use, the design process could also be simplified by automating the controller and sensitivity derivations for future applications of the RFL. All that would be required by the design engineer would be selecting the hydraulic configuration/specifications and entering the flow charts for the selected valves.

BIBLIOGRAPHY

[1] Tulpule, P. J., 2014. "Integrated robust optimal design (irod) via sensitivity minimization". PhD thesis, Iowa State University.

[2] Zhou, H., 2014. "Sensitivity-based robust feedback linearizing control of hydraulically actuated system". Master's thesis, Iowa State University.

[3] Hauser, J., Sastry, S., and Meyer, G., 1992. "Nonlinear control design for slightly non-minimum phase systems: Application to v/stol aircraft". *Automatica,* **28**(4), pp. 665 – 679.

[4] Isidori, A., 1995. *Nonlinear control systems*, Vol. 1. Springer.

[5] Khalil, H. K., and Grizzle, J., 2002. *Nonlinear systems*, Vol. 3. Prentice hall Upper Saddle River.

[6] Ayalew, B., and Jablokow, K. W., 2007. "Partial feedback linearising force-tracking control: implementation and testing in electrohydraulic actuation". *IET Control Theory Applications,* **1**(3), May, pp. 689–698.

[7] h. Kwon, J., h. Kim, T., s. Jang, J., and y. Lee, I., 2006. "Feedback linearization control of a hydraulic servo system". In SICE-ICASE, 2006. International Joint Conference, pp. 455–460.

[8] Spong, M. W., 1987. "Modeling and control of elastic joint robots". *Journal of dynamic systems, measurement, and control,* **109**(4), pp. 310–318.

[9] Gutman, S., 1979. "Uncertain dynamical systems–a lyapunov min-max approach". *Automatic Control, IEEE Transactions on,* **24**(3), pp. 437–443.

[10] Mintsa, H. A., Venugopal, R., Kenne, J. P., and Belleau, C., 2012. "Feedback linearization-based position control of an electrohydraulic servo system with supply pressure uncertainty". *IEEE Transactions on Control Systems Technology,* **20**(4), July, pp. 1092–1099.

[11] Elmali, H., and Olgac, N., 1992. "Robust output tracking control of nonlinear {MIMO} systems via sliding mode technique". *Automatica,* **28**(1), pp. 145 – 151.

[12] Yang, J.-M., and Kim, J.-H., 1999. "Sliding mode control for trajectory tracking of nonholonomic wheeled mobile robots". *IEEE Transactions on Robotics and Automation,* **15**(3), Jun, pp. 578–587.

[13] Chen, H.-M., Renn, J.-C., and Su, J.-P., 2005. "Sliding mode control with varying boundary layers for an electro-hydraulic position servo system". *The International Journal of Advanced Manufacturing Technology,* **26**(1), pp. 117–123.

[14] Kang, H.-J., Kwon, C., Lee, H., and Park, M., 1998. "Robust stability analysis and design method for the fuzzy feedback linearization regulator". *Fuzzy Systems, IEEE Transactions on,* **6**(4), pp. 464–472.

[15] Leland, R. P., 1998. "Feedback linearization control design for systems with fuzzy uncertainty". *Fuzzy Systems, IEEE Transactions on,* **6**(4), pp. 492–503.

[16] Piltan, F., Rezaie, H., Boroom, B., and Jahed, A., 2012. "Design robust backstepping on-line tuning feedback linearization control applied to ic engine". *International Journal of Advance Science and Technology,* **42**, pp. 183–204.

[17] Bode, H., 1952. *Network Analysis and Feedback Amplifier Design.* No. v. 8 in Bell Telephone Laboratories series. Van Nostrand.

[18] Carrigan, J., 2003. "General methodology for multi-objective optimal design of control-structure nonlinear mechanisms with symbolic computing". Master's thesis, Iowa State University.

[19] Bradt, A., 1968. "Sensitivity functions in the design of optimal controllers". *Automatic Control, IEEE Transactions on,* **13**(1), feb, pp. 110 – 111.

[20] Sannuti, P., Cruz, J., Lee, I., and Bradt, A., 1968. "A note on trajectory sensitivity of optimal control systems". *Automatic Control, IEEE Transactions on,* **13**(1), feb, pp. 111 – 113.

[21] Zames, G., 1981. "Feedback and optimal sensitivity: Model reference transformations, multiplicative seminorms, and approximate inverses". *IEEE Transactions on Automatic Control,* **26**(2), Apr, pp. 301–320.

[22] Tulpule, P. J., and Kelkar, A. G., 2013. "Integrated robust optimal design using bmi approach via sensitivity minimization". *J Dyn Syst Meas Control,* **136**(3).

[23] Merritt, H. E., 1967. *Hydraulic control systems*. John Wiley & Sons.

[24] Jelali, M., and Kroll, A., 2012. *Hydraulic servo-systems: modelling, identification and control*. Springer Science & Business Media.

[25] Duffy, J. D., 1998. "A perspective on systems and controls engineering in the earth moving and construction industry". In American Control Conference, 1998. Proceedings of the 1998, Vol. 2, pp. 813–817 vol.2.

[26] Eryilmaz, B., and Wilson, B. H., 2001. "Improved tracking control of hydraulic systems". *Journal of Dynamic Systems, Measurement, and Control,* **123**(3), pp. 457–462.

[27] Vossoughi, G., and Donath, M., 1995. "Dynamic feedback linearization for electro-hydraulically actuated control systems". *Journal of dynamic systems, measurement, and control,* **117**(4), pp. 468–477.

[28] Lim, T., 1997. "Pole placement control of an electrohydraulic servo motor". In Power Electronics and Drive Systems, 1997. Proceedings., 1997 International Conference on, Vol. 1, IEEE, pp. 350–356.

[29] Tang, M., and Chen, L., 2004. "The system bandwidth analysis in electro-hydraulic servo system with pdf control". In Control Conference, 2004. 5th Asian, Vol. 3, IEEE, pp. 1737–1745.

[30] Johnson, P. A., 1996. "Uncertainty of hydraulic parameters". *Journal of Hydraulic Engineering,* **122**(2), pp. 112–114.

[31] Yao, B., Bu, F., Reedy, J., and Chiu, G.-C., 2000. "Adaptive robust motion control of single-rod hydraulic actuators: theory and experiments". *Mechatronics, IEEE/ASME Transactions on,* **5**(1), pp. 79–91.

[32] Wright, W., 1967. "Prediction of bulk moduli and pressure-volume-temperature data for petroleum oils". *ASLE TRANSACTIONS,* **10**(4), pp. 349–356.

[33] Manring, N. D., 1997. "The effective fluid bulk-modulus within a hydrostatic transmission". *J Dyn Syst Meas Control,* **119**, Sep, pp. 462–466.

[34] Wang, J., Gong, G., and Yang, H., 2008. "Control of bulk modulus of oil in hydraulic systems". In Advanced Intelligent Mechatronics, 2008. AIM 2008. IEEE/ASME International Conference on, IEEE, pp. 1390–1395.

[35] Johnston, D., and Edge, K., 1991. "In-situ measurement of the wavespeed and bulk modulus in hydraulic lines". *Proceedings of the Institution of Mechanical Engineers, Part I: Journal of Systems and Control Engineering,* **205**(3), pp. 191–197.

[36] Bongaarts, J., 2009. "Human population growth and the demographic transition". *Philosophical Transactions of the Royal Society of London B: Biological Sciences,* **364**(1532), pp. 2985–2990.

[37] Dimitri, C., Effland, A. B., Conklin, N. C., et al., 2005. *The 20th century transformation of US agriculture and farm policy*, Vol. 3. US Department of Agriculture, Economic Research Service Washington, DC, USA.

[38] Shay, C. W., Ellis, L. V., and Hires, W. G., 1993. "Measuring and reducing soybean harvesting losses". *Extension publications (MU).*

[39] Glancey, J., 1997. "Analysis of header loss from pod stripper combines in green peas". *Journal of agricultural engineering research,* **68**(1), pp. 1–10.

[40] Rehkugler, G., 1970. "Dynamic analysis of automatic control of combine header height". *Transactions of the ASAE,* **13**(2), pp. 225–0231.

[41] Pedersen, P., 2006. *Combine Setting for Minimum Harvest Loss.* Iowa State University Extension.

[42] Briscoe, E., 1953. Automatic control mechanism for cotton harvesters, Nov. 24. US Patent 2,660,015.

[43] and others, 1965. Automatic height control for combine header, Jan. 5. US Patent 3,163,974.

[44] Wright, P. M., 1956. Automatic header control means, June 19. US Patent 2,750,727.

[45] RT, B., 1968. "Automatic header height control for self-propelled combines". *Agricultural Engineering,* **49**(11), p. 666.

[46] Kaminski, T., and Zoerb, G., 1965. "Automatic header-height control for grain crops". *Transactions of the ASAE,* **8**(2), pp. 284–0287.

[47] Lamp, B., Johnson, W., and Harkness, K., 1961. "Soybean harvesting lossesapproaches to reduction".

[48] Lopes, G., Magalhaes, P., and Nóbrega, E., 2002. "Ae–automation and engineering technologies: Optimal header height control system for combine harvesters". *Biosystems engineering,* **81**(3), pp. 261–272.

[49] Jin, C., Shuhong, Z., Yaoming, L., and Jixian, Z., 2003. "Model development and simulation of an automatic height control system for a stripper header [j]". *Transactions of The Chinese Society of Agricultural Engineering,* **6**, p. 025.

[50] YANG, S.-m., YANG, Q., YANG, Y.-h., and YANG, S.-c., 2008. "An ultrasonic-based combine header height control system [j]". *Journal of Agricultural Mechanization Research,* **3**, p. 041.

[51] Gale, G., 1995. "Automatic height control of a stripper harvester using a tactile sensor to detect the crop". *Journal of agricultural engineering research,* **61**(4), pp. 217–226.

[52] Xie, Y., Alleyne, A. G., Greer, A., and Deneault, D., 2013. "Fundamental limits in combine harvester header height control". *Journal of dynamic systems, measurement, and control,* **135**(3), p. 034503.

[53] Xie, Y., and Alleyne, A., 2011. "Integrated plant and controller design of a combine harvester system". In ASME 2011 Dynamic Systems and Control Conference and Bath/ASME Symposium on Fluid Power and Motion Control, American Society of Mechanical Engineers, pp. 819–825.

[54] van der Schaft, A., 1984. "Linearization and input-output decoupling for general nonlinear systems". *Systems & Control Letters,* **5**(1), pp. 27–33.

[55] Henson, M., and Seborg, D., 1990. "Input-output linearization of general nonlinear processes". *Aiche Journal,* **36**(11), Nov, pp. 1753–1757.

[56] Hydraforce valve model numbers. web., Apr, 2015. http://www.hydraforce.com/Modelnos.htm.